AFDELINGEN FOR
BÆRENDE KONSTRUKTIONER
DANMARKS TEKNISKE HØJSKOLE

STRUCTURAL RESEARCH LABORATORY
TECHNICAL UNIVERSITY OF DENMARK

M. W. Bræstrup, M. P. Nielsen, Finn Bach
and B. Chr. Jensen

SHEAR TESTS ON REINFORCED CONCRETE T-BEAMS. SERIES T.

RAPPORT NR. R 72 1976

SHEAR TESTS ON REINFORCED CONCRETE T-BEAMS

SERIES T

by

M.W.Bræstrup, lic.techn.
M.P.Nielsen, dr.techn.
Finn Bach, lic.techn.
B.Chr.Jensen, akademiingeniør

Structural Research Laboratory
Technical University of Denmark

ABSTRACT

The paper reports on 26 shear tests on simply supported T-beams subjected to symmetrical two-point loading. The webs were reinforced by vertical stirrups. The principal variables were the degree of shear reinforcement and the strength of the main reinforcing bars. A few tests with different stirrup arrangements were included.

With the purpose of investigating the shear failure mechanism, the rotation of the beam end over the support was measured, and two beams were cut through at normal sections to reveal the interior cracking.

The principal conclusions drawn from the tests are as follows:

- The failure mechanism consists of a translation of the loaded section with respect to the supported section, without any rotation of the beam end;
- The ultimate load is independent upon the strength of the main reinforcement, provided it is strong enough to ensure a proper shear failure;
- The ultimate load is independent upon the degree of shear reinforcement, when the latter is sufficiently high;
- The ultimate load is in good agreement with the web crushing criterion based upon the theory of plasticity (cf. Chapter 1 and references [1]-[4]).

TABLE OF CONTENTS

INTRODUCTION

Dating back to the spring of 1973, a theoretical and experimental study of the shear strength of reinforced concrete beams is being carried out at the Structural Research Laboratory of the Technical University of Denmark. The project is sponsored by the Danish Council for Scientific and Technical Research, which has granted funds for three years of experimental investigation.

The purpose of the present paper is to report on series T, the first test series of this programme, consisting of 26 beams, which were tested to failure in the fall of 1973 and the spring of 1974. The specific aim of series T was to study an expression for the ultimate shear load based upon plastic analysis, and to investigate the relevance of the corresponding failure mechanism. The theory was originally proposed by NIELSEN [1], [2] as a lower bound for the load-carrying capacity when web failure is critical. Later it was shown, NIELSEN & BRÆSTRUP [3] , BRÆSTRUP [4], that the web crushing criterion is also an upper bound, thus establishing it as the correct plastic solution for the shear strength.

The report gives an analysis of the tests in general, exemplified by a specific beam. In addition, the report contains a rather detailed description of test procedure and equipment, which is used almost unchanged for the subsequent test series of the programme. Readers mainly concerned with the results may skip chapters 2, 3, and 4, except for the references to tables and figures made in chapter 5.

Its bulkiness notwithstanding, the report does not contain all the relevant material. The laboratory reports, photographs, and computer output corresponding to the 26 individual beam tests are filed at the Laboratory. This unpublished appendix also contains the analysis of the four concrete cylinders equipped with strain gauges, as well as all the computer programmes described in the report.

TABLES AND FIGURES

The tables and figures are numbered consecutively within each section. Below they are listed with page numbers for easy reference.

Tables

Figures

NOTATIONS

The symbols are defined when they first occur in the text. The frequently used notations are listed alphabetically below.

A : Cross-sectional area of longitudinal bottom reinforcement

A_o : Cross-sectional area of longitudinal top reinforcement

a : Shear span

b : Web width

b_s : Interior width of stirrup hoops

b_o : Flange width

C : Compressive stringer force

d : Depth from top of beam to centroid of main reinforcement

d_o : Depth from top of beam to centroid of top reinforcement

E_ℓ : Elastic modulus for longitudinal concrete strains

E_s : Elastic force-strain modulus for steel bar

E_t : Elastic modulus for transverse concrete strains

h : Beam depth

h_s : Depth of web from bottom of flange to centroid of the lower layer of main reinforcement

h_w : Depth of web from bottom of flange to centroid of main reinforcement

h_o : Flange depth

h^* : Effective shear depth

M_F : Flexural failure moment of beam

N : Number of tests in a series (sample)

N_a : Force in longitudinal tension reinforcement

N'_a : Force in longitudinal compression reinforcement

N'_b : Force in concrete compression zone

N'_{bo} : Compressive force in concrete flange

P : Applied load

P_F : Flexural failure load of beam

P_u : Ultimate load of steel bar

P_Y : Yield load of steel bar

r : Instantaneous radius of rotation of beam end

s : Equivalent stirrup stress. Standard deviation based upon (N-1) degrees of freedom

s_y : Equivalent stirrup yield stress
u : Elongation of main reinforcement in shear span
V : Shear force
V_{cr} : Shear cracking load
V_u : Ultimate shear load
V_w : Shear force carried by web
V_o : Shear force carried by flange
v : Deflexion of loaded section of beam
w : Compression of flange in shear span
x : Depth to neutral axis
y : Depth of rectangular stress block
z : Internal moment lever arm

α : Curving of bending span
Δ : Prefix indicating increment between two scans
δ : Deformation rate. Coefficient of variation
ε_a : Strain in longitudinal tension reinforcement
ε'_a : Strain in longitudinal compression reinforcement
ε'_{bu} : Compressive concrete failure strain i flexure
ε_F : Uniaxial compressive concrete failure strain
ε_ℓ : Longitudinal strain of concrete cylinder
ε_t : Transverse strain of concrete cylinder
ε_u : Ultimate strain of steel bar
ε_y : Yield strain of steel bar
θ : Inclination of yield lines
λ : Ratio of shear span to shear depth
ν : Web effectiveness ratio
σ_b : Compressive concrete stress
σ_c : Compressive concrete cylinder strength
σ_c^* : Effective web strength
σ_t : Tensile concrete strength
τ : Nominal shear stress of beam
τ_F : Nominal shear stress at flexural failure of beam

φ : Inclination of concrete web compression

ψ : Degree of shear reinforcement

ψ_o : Degree of shear reinforcement corresponding to flattest possible yield line

ψ_1 : Lowest degree of shear reinforcement for which the beam is over-reinforced in shear

1. THEORETICAL BACKGROUND

1.1 The web crushing criterion

The analysis is based upon the assumptions listed below:

(a) The beam is in a plane state of stress.

(b) The compression zone and the main longitudinal reinforcement act as stringers with compression and tension, respectively.

(c) The stirrup material is rigid, perfectly plastic, and the stirrups are unable to resist lateral forces. The spacing of the stirrups is sufficiently close to permit a description of their action by the equivalent stirrup stress s, per unit area perpendicular to the stirrup direction. At yield $s = s_y$.

(d) The concrete of the web is rigid, perfectly plastic with the square (modified COULOMB) failure criterion as yield locus and with the associated flow rule. The tensile strength is zero and the compressive strength is $\sigma_c^* = \nu\sigma_c$, where σ_c is the cylinder strength, and ν is the web effectiveness ratio.

Under these assumptions, the shear strength of a simple beam with vertical stirrups is given by the web crushing criterion (cf. reference [3])

$$V = bh^* s_y \sqrt{\frac{\sigma_c^*}{s_y} - 1} \tag{1a}$$

Here:

V is the applied shear force
b is the width of the web
h^* is the effective shear depth

Equation (1a) may be stated on non-dimensional form as:

$$\tau/\sigma_c = \sqrt{\psi(\nu - \psi)} \tag{2a}$$

where we have introduced the nominal shear stress τ and the shear reinforcement degree ψ :

$$\tau = \frac{V}{bh^*} \quad , \quad \psi = \frac{s_y}{\sigma_c}$$

Equation (2a) is valid for $\psi \leq \nu/2$. For $\psi > \nu/2$ the shear strength is:

$$V = \frac{1}{2} bh^* \sigma_c^* \tag{1b}$$

or:

$$\tau/\sigma_c = \nu/2 \tag{2b}$$

The shear strength given by equation (2a) is the maximum lower bound corresponding to a homogeneous state of stress with yielding of the stirrups and a uniaxial compression σ_c^* in the web concrete, inclined at the angle φ to the beam axis (cf. Figure 1.1.1). The stress distribution is modified in regions below the load and over the support (cf. reference [3]). The angle φ is given by:

$$\cot\varphi = \sqrt{\nu/\psi - 1} \qquad \text{for} \qquad \psi \leq \nu/2$$

$$\cot\varphi = 1 \qquad \text{for} \qquad \psi > \nu/2$$

In the latter case the beam is overreinforced, i.e. the stirrups are not yielding at failure of the beam. The shear strength is then given by equation (2b).

Equations (2) are also the minimum upper bound corresponding to a failure mechanism with vertical displacement rates in diagonal yield lines. The inclination of the yield lines is $\theta = 2\varphi$. The failure mechanism is shown on Figures 1.1.1a and b, for concentrated and distributed strain rates, respectively.

The failure mechanism requires $\cot\theta \leq \lambda$, where $\lambda = a/h^*$

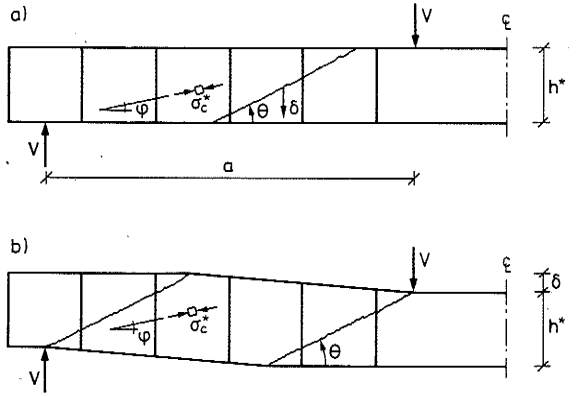

Figure 1.1.1: Shear failure mechanism

a) Concentration strain rates
b) Distributed strain rates

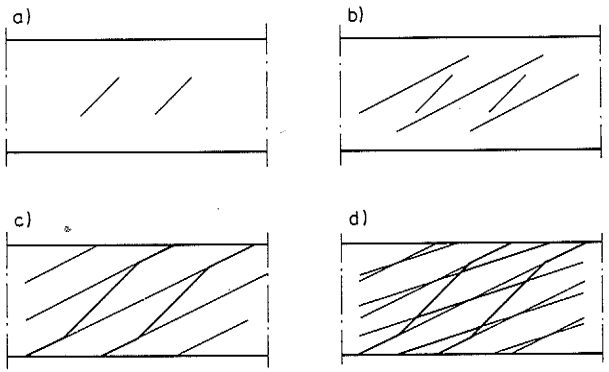

Figure 1.1.2: Development of web cracking

a) Stage I : The first cracks are formed
b) Stage II : The cracks become flatter
c) Stage III: Yield lines are formed
d) Stage IV : The yield lines become flatter

and a denotes the length of the shear span. Thus equation (2a) is only an upper bound provided $\psi \geq \psi_o$, where

$\psi_o = \frac{\sqrt{1+\lambda^2}-\lambda}{2\sqrt{1+\lambda^2}} \nu$. For a shear span ratio of $\lambda=3$, we get $\psi_o = 0.0256\ \nu$. This degree of shear reinforcement is too small to be of interest for the beams of series T.

The main difference between the proposed theory and the usual shear-compression theories, is that the failure mechanism does not involve any rotation about a plastic hinge. Consequently, shear stresses are transferred across the diagonal yield lines.

In order to be specific, it is convenient to distinguish between cracks and yield lines. Cracks develop in the direction of the principal compressive concrete stress, and they need not be accompanied by any significant deformations. The deformations take place in yield lines, which in general do not follow the trajectories of principal stress.

The behaviour of a non-prestressed beam during loading to shear failure, as predicted by the theory, is as stated below and shown schematically on Figure 1.1.2:

I : The first cracks follow the trajectories of principal stress in the uncracked beam, i.e. their inclination is roughly equal to 45^o (Figure 1.1.2a).

II : As the stirrups are activated, the inclination of the subsequent cracks decreases (Figure 1.1.2b).

III: The cracks are joined into yield lines of steeper inclination and carrying shear (Figure 1.1.2c).

IV : A further increase of load results in a flattening of the yield lines, activating more stirrups (Figure 1.1.2d). This process continues until the compressive stress in the web concrete reaches the strength limit. The failure may appear as actual web crushing, or it may lead to excessive deformations, causing the destruction of the compression flange.

1.2 Application of the theory

In order to be able to use the web crushing criterion, equations (2), for analysis and design, we need to assess the values of the quantities h^* and $\nu = \sigma^*/\sigma_c$.

There are at least two reasons why the web effectiveness ratio ν must be less than unity. Firstly, the state of stress in the web is not plane, as required by assumption (a) of the preceding section. The forces from the stirrups are transferred to the main reinforcing bars, which in turn are supported by the web concrete. Thus the web compression is concentrated at the longitudinal bars, see Figure 1.2.1, and this concentration gives rise to failure before the average stress in the web reaches the uniaxial compressive concrete strength. Secondly, because of the limited deformability of the concrete and the unstable nature of concrete failure, we cannot expect the concrete stress to equal the maximum compressive strength at all points of the yield lines at failure.

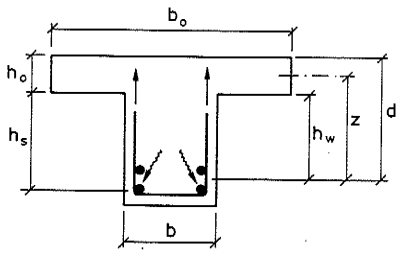

Figure 1.2.1: Illustration of effective web strength and effective shear depth

An assessment of the web effectiveness ν by comparing the web crushing criterion, equations (2), with experimental results from shear tests, is influenced by the choice of effective shear depth h^*. The depth h^* is the distance between tension and compression stringers. For T-beams we may take the latter to be identical with the compression flange, but even so there are a number of ways of defining the shear depth, as illustrated on Figure 1.2.1. The usual practice is to relate the nominal shear stress to the effective depth d. The Danish Code of Practice puts the shear depth equal to the internal moment lever arm z. Most in line with the proposed theory, would be to use the depth h_w (or h_s), i.e. the distance from the centroid of the main reinforcement (or from the lower layer of bars) to the bottom of the compression zone. This is the depth of the concrete body which is supposed to be resisting the shear force. It must be stressed that the assumed identity of compression zone and flange is only meaningful, provided the flange is designed to be necessary and sufficient to resist the compressive stringer force.

Most building codes include a contribution V_o from the compression zone to the total shear resistance. However, if the flange is used to its full capacity to resist the compressive stringer force, it cannot be carrying shear as well.

If there is shear in the flange, this contribution may conveniently be included in the effective shear depth. Figure 1.2.2a shows a section dx of the compression zone with depth h_o. The compressive force C decreases towards the support as the shear stress τ is transferred to the web. Moment equilibrium yields:

$$V_o dx = C \cdot \frac{1}{2} h_o - (C - \tau b\, dx) \frac{1}{2} h_o$$

$$V_o = \frac{1}{2} \tau b\, h_o$$

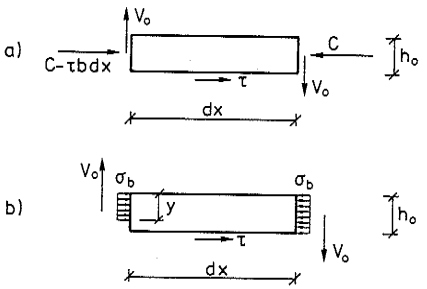

Figure 1.2.2: Flange shear contribution

a) Central compressive force
b) Compressive force concentrated in upper fibres

Denoting the web shear by V_w, we find the total shear resistance:

$$V = V_w + V_o = \tau b\, h_w + \frac{1}{2}\tau b\, h_o = \tau b h^* \quad ,$$

where the effective shear depth is $h^* \approx h_w + \frac{1}{2}h_o = z$. Thus the flange shear is included if the shear depth is put equal to the internal moment lever arm, as required by the Danish Code of Practice.

The analysis given above rests on the assumption that the stringer force continues to act in the centre of the flange as it decreases through the shear span. We might as well assume the compressive force to be concentrated in the top fibres of the flange, the concrete stress σ_b remaining constant, see Figure 1.2.2b. Moment equilibrium now yields:

$$V_o dx = C\,\frac{1}{2}h_o - (C - \tau b dx)\,(h_o - \frac{1}{2}y) \quad ,$$

where the depth y of the compressive zone is given by the equation

$$\sigma_b = \frac{C - \tau b dx}{y b_o} = \frac{C}{h_o b_o} \quad ,$$

b_o being the width of the flange. Hence we find:

$$V_o dx = \frac{1}{2} C h_o - (C - \tau b dx)\left(h_o - \frac{1}{2} h_o + \frac{1}{2} \frac{\tau b h_o dx}{C}\right)$$

$$= \frac{1}{2} \frac{h_o}{C} (\tau b dx)^2$$

i.e $V_o \approx 0$.

Thus under those assumptions we get no contribution from the compression flange. Presumably, the truth lies somewhere in between, and as discussed in reference [3] the available test data does not permit a conclusion. Therefore we shall tentatively use the internal moment lever arm as effective shear depth.

2. TEST PLANNING

2.1 Purpose of the tests

Because of the parameters h^* and ν, an experimental verification of equations (2) will always be open to discussion. It is straightforward, however, to test the validity of certain features of the theory, especially the failure mechanism. Therefore the purpose of the test series is as follows:

(1) To verify that at failure the deformations consist of pure shearing, without rotation of the beam end over the support.

(2) To verify that the shear strength is independent of the strength of the main reinforcement.

(3) To verify that for sufficiently strong shear reinforcement ($\psi > \nu/2$), the failure load is independent of the shear reinforcement.

(4) To assess the magnitude of the effective shear depth h^* and the web effectiveness ν.

As explained in the preceding section, the effective web strength σ_c^* is supposed to depend on the arrangement of the reinforcement. A few pilot tests are included in series T, but a detailed investigation of this question is undertaken by subsequent test series.

In order to achieve the objectives (1)-(4) stated above, it is necessary to collect experimental data from beams covering a wide range of shear reinforcement strengths. Thus the desirable interval of variation for the shear reinforcement degree ψ is something like $0 < \psi < 1$. Shear reinforcement strengths $\psi > 0.5$ are hard to obtain, however, without making the web width b very small. Therefore tests of this type are usually carried out on thin-webbed I-beams. On the other hand, a substantial web width is necessary in order to permit any investigation of the influence of concrete cover and stirrup layout. It was therefore decided that the web width should be $b = 200$ mm. For such beams, shear reinforcement degrees $\psi > 0.2$ are rarely seen, because stronger shear reinforcement

would normally lead to flexural failure. To be able to study shear failures with strong shear reinforcement, we adopted the measures listed below:

- Low concrete strength
- Big compression flange
- High strength longitudinal reinforcement.

and for the most strongly reinforced beams:

- High strength stirrup reinforcement.

As a consequence, it should be stressed that the test beams are not representative of practical design and the results are primarily of theoretical interest. The philosophy behind this approach is that once the theory has been tested under such extreme conditions, it may be used with confidence in practical cases. If we confine ourselves to the conventional parameter ranges, the results get so blurred by random test variations, that any theory may be brought to agreement, as is amply demonstrated in the literature.

2.2 Beam types and identifications

Each beam is given a beam number, e.g. Beam No.T6018 m, constituted by a series identification (upper case letter), a specimen number (four digits), and possibly a type identification (lower case letter).

The beam of series T had a nominal *) concrete strength of $\sigma_c = 110$ kp/cm^2 and the main reinforcement consisted of six

*) The term 'nominal' is used to designate a formal value, in this case the strength attempted by the design of the concrete mix. Thus the concept does not imply that safety factors have been introduced.

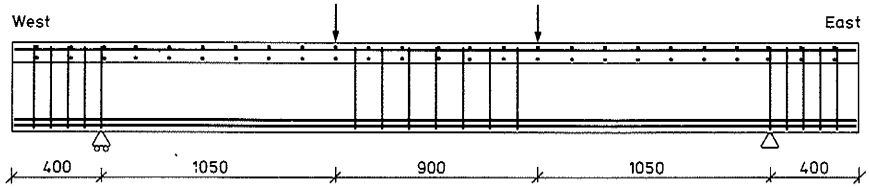

Figure 2.2.1: Elevation of test beam
(normal type and type d)
Variable stirrup reinforcement
not shown.

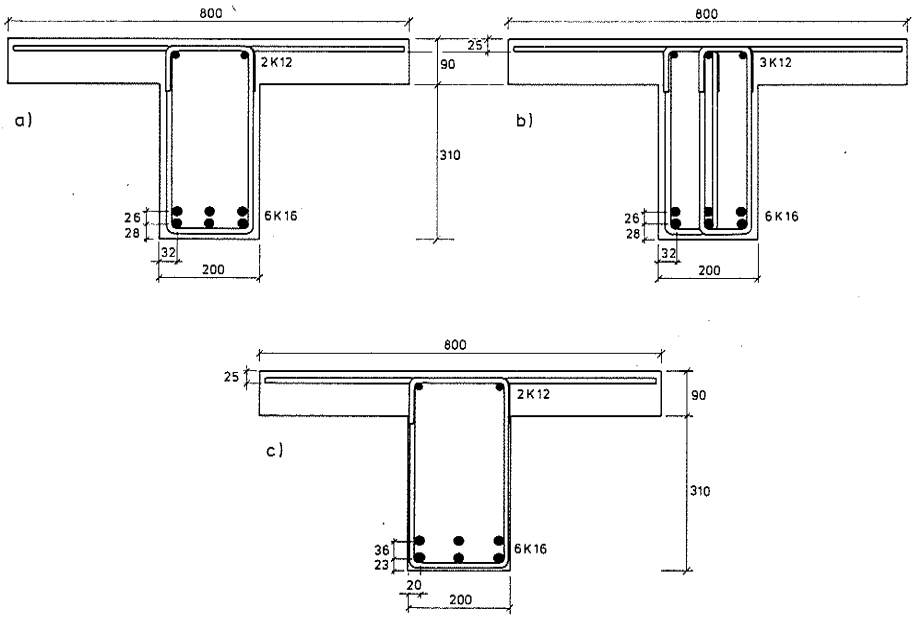

Figure 2.2.2: Normal sections of test beams

a) Normal beam type
b) Beam type d
c) Beam type m

16 mm diameter deformed bars (K 16) arranged in two layers. The beam is shown in elevation on Figure 2.2.1. The overall length is 3800 mm, comprising the following zones:

Anchorage zone west:	400 mm
Shear span west:	1050 mm
Bending span:	900 mm
Shear span east:	1050 mm
Anchorage zone east:	400 mm

Thus the distance between the supports is 3000 mm, and the distance between the symmetrical point loads is 900 mm. The total depth is 400 mm, and the effective depth is 359 mm, the shear span/depth ratio being $a/d = 2.92$.

The beam type refers to the arrangement of the reinforcement. No lower case letter at the end of the beam number indicates that the beam is of the common type, with a normal section as shown on Figure 2.2.2a. The stirrups were bent around the 12 mm diameter (K 12) top reinforcement, the overlap consisting of the upper horizontal leg and approximately 80 mm of the vertical legs.

Beam types d and m were designed to reveal the influences of stirrup layout and concrete cover, respectively. Figure 2.2.2b shows the normal section of type d where the double stirrups were arranged as two narrow stirrups in such a way that all three bars of the lower reinforcement layer were supported by stirrup bends. Beam type m , shown on Figure 2.2.2c, had only half the concrete cover to the side of the main reinforcement. The two layers of bars were separated a little to make room for the dial gauge holders (cf. section 3.5), the effective depth remaining unchanged.

The beam specimen number furnishes information on the strength of main and shear reinforcement. In order to study the influence of main reinforcement strength, three different steel qualities were used. The first two digits of the specimen number indicate the nominal yield stress (in kp/mm^2) of the main reinforcing bars.

The last two digits of the number represent the nominal shear reinforcement degree ψ (in 10^{-2}) . The actual value of ψ is somewhat different, mainly due to variations of concrete strength (cf. section 3.2). The stirrup reinforcement corresponding to each specimen number is listed in Table 2.2.1, which also indicates the main steel qualities used with each stirrup reinforcement. The table contains 22 beams, the remaining four being Beams Nos. T6018 and T9029 designed as types d and m .

Specimen number	Stirrup reinforcement	Main steel quality	Specimen number	Stirrup reinforcement	Main steel quality
05	R6/131	- 60 -	36	2R10/105	- - 90
10	2R6/131	- 60 -	40	2R10/96	- - 90
14	2R6/96	52 60 -	43	2R10/87.5	- - 90
18	2R10/210	52 60 -	47	2R10/81	- - 90
22	2R10/175	52 60 -	60	2S10/150	- - 90
25	2R10/150	- 60 90	65	2S10/131	- - 90
29	2R10/131	- 60 90	71	2S10/117	- - 90
32	2R10/117	- 60 90	78	2S10/105	- - 90

Table 2.2.1: Key to stirrup reinforcements

Three different types of stirrup reinforcement were used: 6 mm smooth mild steel bars (R6), 10 mm smooth steel bars (R10), and 10 mm smooth cold-worked bars (S10). With the exception of Beam No.T6005, the shear reinforcement was placed as double stirrups, and the number preceded by a stroke indicates the stirrup spacing in mm. Thus the notation 2R10/81 means that pairs of 10 mm diameter mild steel stirrups are placed at a distance of 81 mm. The shear span of 1050 mm is a multiplum of the distances between the (pairs of) stirrups, and the distance from the load or from the support to the nearest stirrup is half the stirrup spacing.

2.3 Flexural design

The load-carrying capacity of the beams in flexion is found using a rectangular stress block of depth $y = 3/4\ x$, x being the neutral axis depth (cf. BRØNDUM-NIELSEN [5] p.66 ff.). The properties listed below are common to all beams:

Shear span	$a = 105$ cm
Nominal concrete strength	$\sigma_c = 110$ kp/cm^2
Bottom steel area	$A = 12.06$ cm^2
Top steel area	$A_o = 2.26$ cm^2 *)
Total depth	$h = 40$ cm
Flange depth	$h_o = 9$ cm
Web width	$b = 20$ cm
Flange width	$b_o = 80$ cm
Effective depth to tension steel	$d = 35.9$ cm
Distance from top of beam to top steel	$d_o = 3.1$ cm
Internal moment lever arm	$z = 31.4$ cm

*) The beams of series Td had $A_o = 3.39$ cm^2

The compression steel has a nominal yield stress of 4200 kp/cm^2. The force in the compression reinforcement, assuming yield, is $N'_a = 9500$ kp (14250 kp for series Td). The concrete compressive failure strain in flexion is assumed to be $\varepsilon'_{bu} = 3.5‰$.

For the beams T52 the nominal yield force of the main reinforcement is $N_a = A \cdot 5200 = 62700$ kp . The force to be delivered by the concrete compression zone is $N'_b = N_a - N'_a = 53200$ kp. Hence the depth of the rectangular stress block is:

$$y = \frac{N'_b}{b_o \sigma_c} = \frac{532000}{80 \cdot 110} = 6.0 \text{ cm} \quad ,$$

the neutral axis depth being $x = \frac{4}{3}y = 8.1$ cm.

The strains of the tension and compression reinforcements are:

$$\varepsilon_a = \frac{d-x}{x}\,\varepsilon'_{bu} = \frac{35.9-8.1}{8.1} \cdot 3.5 = 12.0\% ,$$

and $$\varepsilon'_a = \frac{x-d_o}{x}\,\varepsilon'_{bu} = \frac{8.1-3.1}{8.1} \cdot 3.5 = 2.2\% .$$

These strains are great enough to ensure yield of the steel as assumed.

The ultimate flexural moment is

$$M_F = N'_a(d-d_o) + N'_b(d-\tfrac{1}{2}y)$$

$$= 9500(35.9-3.1) + 53200(35.9-3.0)$$

$$= 3.1 \cdot 10^5 + 17.5 \cdot 10^5 = 20.6 \cdot 10^5 \text{ kpcm}$$

the flexural failure load being

$$P_F = \frac{M_F}{a} = \frac{20.6 \cdot 10^2}{105} = 19.6 \text{ Mp}$$

The maximum shear stress τ_F at flexural failure is given by:

$$\tau_F/\sigma_c = \frac{P_F}{bz\,\sigma_c} = \frac{19600}{20 \cdot 31.4 \cdot 110} = 0.284$$

For the beams T60, we find:

$$N_a = A \cdot 6000 = 72400 \text{ kp}$$

$$N'_b = N_a - N'_a = 62900 \text{ kp}$$

$$y = \frac{N'_b}{b_o \tau_c} = \frac{62900}{80 \cdot 110}\text{cm} = 7.1 \text{ cm} \qquad x = \frac{4}{3}y = 9.5 \text{ cm}$$

$$\varepsilon_a = \frac{d-x}{x}\varepsilon'_{bu} = \frac{35.9-9.5}{9.5}\,3.5 = 9.7\%$$

$$\varepsilon'_a = \frac{x-d_o}{x}\varepsilon'_{bu} = \frac{9.5-3.1}{9.5}\,3.5 = 2.4\%$$

$$M_F = N'_a(d-d_o) + N'_b(d-\tfrac{1}{2}y)$$

$$= 3.1\cdot10^5 + 62900(35.9-3.6) = 23.4\cdot10^5 \text{ kpcm}$$

$$P_F = \frac{M_F}{a} = \frac{23.4\cdot10^2}{105} = 22.3 \text{ Mp}$$

$$\tau_F/\sigma_c = \frac{P_F}{bz\sigma_c} = \frac{22300}{20\cdot31.4\cdot110} = 0.323$$

Finally, for beams T90:

$$N_A = A\cdot9000 = 108500 \text{ kp}$$

$$N'_b = N_a - N'_a = 99000 \text{ kp}$$

The maximum compressive force that can be resisted by the flange concrete alone is:

$$N'_{bo} = h_o b_o \sigma_c = 9\cdot80\cdot110 = 79200 \text{ kp} < N'_b$$

Hence:

$$y = h_o + \frac{N'_b - N'_{bo}}{b\sigma_o} = 9.0 + \frac{99000-79200}{20\cdot110} = 18.0 \text{ cm}$$

$$x = \frac{4}{3}y = 24.0 \text{ cm}$$

$$\varepsilon_a = \frac{d-x}{x}\,\varepsilon'_{b_u} = \frac{35.9-24.0}{24.0}\cdot 3.5 = 1.7\%$$

$$\varepsilon'_a = \frac{x-d_o}{o}\,\varepsilon'_{b_u} = \frac{24.0-3.1}{24.0}\cdot 3.5 = 3.0\%$$

The tensile strain is too small to warrant the assumption that the main steel is yielding. Thus the calculated value of the ultimate flexural moment will be slightly unconservative:

$$M_F = N'_a(d-d_o) + N'_{bo}(d-\tfrac{1}{2}h_o) + (N'_b-N'_{bo})(d-\tfrac{1}{2}h_o-\tfrac{1}{2}y)$$

$$= 3.1\cdot10^5 + 79200(35.9-4.5) + 19800(35.9-4.5-9.0)$$

$$= 32.4\cdot10^5 \text{ kpcm}$$

$$P_F = \frac{M_F}{a} = \frac{32.4\cdot10^2}{105} = 30.9 \text{ Mp}$$

$$\tau_F = \frac{P_F}{bz\sigma_c} = \frac{30900}{20\cdot31.4\cdot110} = 0.447$$

The actual strengths of concrete and reinforcement for each beam are given in Chapter 3. Using these strength parameters, the flexural capacities of the beams are calculated by the computer programme FLEX (cf. Section 4.1). The results are listed in Table 2.3.1. Note that at flexural failure the concrete compression zone extends into the web for most of the beams, and that all the beams T90 are overreinforced in flexion.

CALCULATION OF:

Y: DEPTH OF RECTANGULAR STRESS BLOCK EPSA: TENSILE REINFORCEMENT STRAIN

EPSAO: COMPRESSIVE REINFORCEMENT STRAIN PF: FLEXURAL FAILURE LOAD

FOR BEAMS WITH:

SHEAR SPAN A TENSILE REINFORCEMENT: NRA BARS AT DEPTH D WITH YIELD STRAIN EPSAY AND WITH YIELD FORCE PAY

WEB WIDTH B COMPRESSIVE REINFORCEMENT: NRAO BARS AT DEPTH DO WITH YIELD STRAIN EPSAYO AND WITH YIELD FORCE PAYO

FLANGE WIDTH BO

FLANGE DEPTH HO CONCRETE COMPRESSIVE STRENGTH SIGMAC CONCRETE FAILURE STRAIN EPSBY

DATA COMMON TO ALL BEAMS:

A= 105.0 CM B= 20.0 CM BO= 80.0 CM HO= 9.0 CM D= 35.9 CM DO= 3.1 CM

EPSAYO= 2.2 0/00 PAYO= 5200. KP EPSBY= 3.5 0/00

BEAM NO.	SIGMAC KP/SQCM	NRA	EPSAY 0/00	PAY MP	NRAO	Y CM	EPSA 0/00	EPSAO 0/00	PF MP
T5214	109.	6	2.7	11.6	2	6.8	10.4	2.3	21.6
T5218	105.	6	2.8	11.3	2	6.8	10.3	2.3	21.0
T5222	105.	6	2.8	11.3	2	6.8	10.3	2.3	21.0
T6005	108.	6	3.3	14.8	2	7.6	9.6	2.3	21.5
T6010	105.	6	3.4	14.9	2	10.6	6.6	2.8	26.7
T6014	110.	6	3.5	14.8	2	10.6	5.4	2.7	26.7
T6018	112.	6	3.5	14.8	2	8.4	7.7	2.5	26.0
T6022	106.	6	3.4	14.8	2	8.7	7.3	2.6	26.0
T6026	105.	6	3.4	14.8	2	10.0	5.9	2.7	26.6
T6029	108.	6	3.4	14.8	2	10.3	5.6	2.7	26.6
T6032	120.	6	3.4	14.6	2	8.1	8.0	2.5	26.7
T9025	128.	6	3.3	14.6	2	8.0	8.2	2.5	26.7
T9029	81.	6	4.3	18.4	2	12.6	4.7	2.5	32.7
T9032	101.	6	4.5	18.6	2	14.3	3.1	3.3	32.4
T9036	102.	6	4.3	18.4	2	13.3	3.6	3.1	27.0
T9040	116.	6	4.3	18.4	2	12.9	3.8	3.1	28.1
T9043	105.	6	4.3	18.4	2	12.6	4.0	3.0	30.6
T9047	120.	6	4.4	18.5	2	13.1	3.7	3.1	27.9
T9050	121.	6	4.3	18.7	2	12.9	4.3	2.8	32.9
T9065	102.	6	4.3	18.4	2	12.6	4.1	2.9	31.2
T9071	111.	6	4.3	18.4	2	13.2	3.6	3.1	27.2
T9078	116.	6	4.3	18.4	2	13.6	3.0	3.0	29.1
T6018D	98.	6	3.4	14.8	3	12.6	4.0	3.0	30.6
T9029D	110.	6	3.3	14.8	3	10.3	5.6	2.7	26.6
T6018N	107.	6	3.4	14.8	2	12.5	4.0	3.0	30.4
T9029N	116.	6	4.2	17.9	2	12.5	4.0	2.7	28.5
								3.0	30.2

Table 2.3.1: Flexural analysis of test beams

2.4 Design of shear and secondary reinforcement

The shear reinforcement is designed to cover a broad range of strengths. The stirrup reinforcements used are listed in Table 2.2.1 of the preceding section and displayed on Figure 2.4.1. The two curves represent the web crushing criterion with $\nu = 0.65$ and $\nu = 0.80$. Thus the shaded region between the curves are the points where shear failures are to be expected. The beams listed in Table 2.2.1 are represented by vertical lines at the nominal shear reinforcement parameters. The horizontal lines correspond to flexural failure of the beams T52, T60, and T90 , respectively. The nominal flexural failure loads of the 22 beams are marked with dots. On the figure it is noted that all the beams T90 are designed to fail in shear, whereas some of the beams T52 and T60 may be expected to get flexural failure.

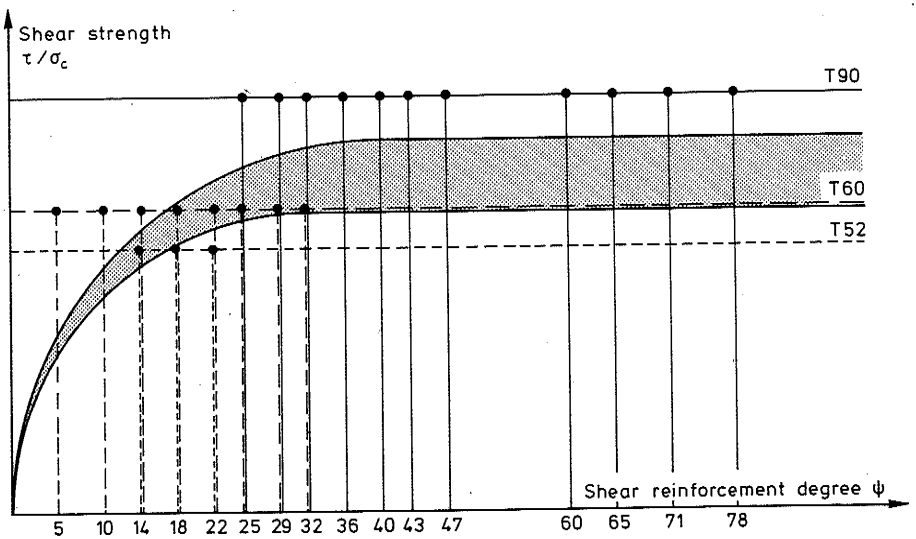

Figure 2.4.1: Expected shear and flexural strength of test beams

To prevent failure of the anchorage of the main reinforcement, the beam was extended 400 mm beyond the support, and five mild steel stirrups of diameter 8 mm were provided. Seven identical stirrups were placed in the bending span to reinforce it against shear during the second shear test of the beam (cf. Section 3.5. For some beams only five stirrups were used, but it proved to be insufficient, see Section 4.2). The secondary stirrup reinforcement is shown on Figure 2.2.1.

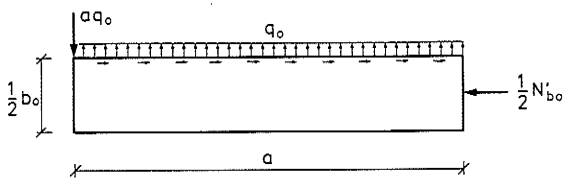

Figure 2.4.2: Equilibrium of one half of flange of shear span

As the compressive force in the flange declines from the load towards the support, shear is transferred to the web. At the vertical section between web and flange, this shear must be resisted by a transverse flange reinforcement. A rough estimate of the tensile force this reinforcement is subjected to may be obtained considering one half of the flange, Figure 2.4.2, neglecting the width of the web. The maximum compressive force carried by half the flange at the loaded section is $\frac{1}{2}N'_{bo} = \frac{1}{2}b_o h_o \sigma_c$, which is assumed to be reduced to zero at the support. We assume the transverse tensile force to be uniformly distributed, of magnitude q_o per unit length, and to be balanced by a compressive force aq_o , acting at the support. Moment equilibrium yields:

$$aq_o \cdot \frac{1}{2}a = \frac{1}{2}N'_{bo} \cdot \frac{1}{4}b_o$$

i.e.

$$q_o = \frac{1}{4}\left(\frac{b_o}{a}\right)^2 h_o \sigma_c = \frac{1}{4}\left(\frac{80}{105}\right)^2 9 \cdot 110 = 144 \text{ kp/cm}$$

The same value is given by BRØNDUM-NIELSEN [5] pp.162 ff. as the maximum tensile force. He assumes a parabolic variation of the compressive flange force and a parabolic thrust line, and considers transverse equilibrium along the shear span. The solution, however, does not satisfy moment equilibrium.

Taking into account the area required to resist the compressive force aq_o and requiring it to belong to the shear span, the value of q_o becomes slightly higher (168 kp/cm).

The transverse flange reinforcement consisted of two 8 mm diameter mild steel bars per 15 cm. Taking the yield stress of the steel to be 2700 kp/cm^2, the yield force per unit length is $2700 \text{ kp/cm}^2 \cdot \frac{1 \text{ cm}^2}{15 \text{ cm}} = 180 \text{ kp/cm}$. The transverse reinforcement is provided all along the beam and shown on Figures 2.2.1 and 2.

3. TEST EXECUTION

3.1 Manufacturing and curing

Table 3.1.1: Distribution of main and shear reinforcement

Beam Number	Main Reinf.	Stirrup Reinf. EAST	Stirrup Reinf. WEST	Beam Number	Main Reinf.	Stirrup Reinf. EAST	Stirrup Reinf. WEST
T5214	5201 5202	1 620 3 614 4 615$_4$ 7 616$_3$ 7 617^3	2 620 3 614 3 615$_2$ 7 618^1 7 619^1	T9032	9007 9008 9009	1 1011 1 1012$_3$ 8 1019^3 8 1010^4	1 1009 1 1010$_1$ 8 1017^1 8 1018^2
T5218	5203 5204	5 1041$_4$ 5 1042^3	1 1041 1 1042$_2$ 8 1043^2 8 1044$_1$	T9036	9010 9010 9012	2 1005 2 1006$_4$ 8 1021^4 8 1022^3	2 1007 2 1008$_2$ 8 1023^2 8 1024^1
T5222	5205 5206	4 1066$_4$ 8 1064^3	4 1066$_2$ 8 1065$_1$	T9040	9013 9014 9015	3 1002$_3$ 3 1001^3 8 1025$_4$ 8 1026	3 1003$_2$ 3 1004^1 8 1027^1 8 1028
T6005	6001 6002	1 603$_3$ 7 601$_4$	1 603$_1$ 7 602$_2$	T9043	9016 9017 9018	4 1029 4 1030$_4$ 8 1031^3 8 1032^3	4 1029 4 1030$_2$ 8 1033^1 8 1034^1
T6010	6003 6004	2 603$_4$ 7 604^3 7 605^3	2 603$_2$ 7 606^1 7 607^1	T9047	9019 9020 9021	1 1041 1 1042 4 1035 4 1036$_4$ 8 1037^3 8 1038^3	1 1041 1 1042 4 1035 4 1036$_2$ 8 1039^1 8 1040^1
T6014	6005 6006	1 603 1 614 3 610 3 611$_4$ 7 608^3 7 609^3	4 610 4 611$_2$ 7 612^1 7 613^1	T9060	9037 9038 9039	14 S10	14 S10
T6018	6007 6008	5 1001^4 5 1002^3	5 1003^2 5 1004^1	T9065	9034 9035 9036	16 S10	16 S10
T6022	6009 6010	6 1005^4 6 1006^3	6 1007^2 6 1008^1	T9071	9028 9029 9030	18 S10	18 S10
T6025	6011 6012	7 1044^4 7 1045^3	7 1046^2 7 1047^1	T9078	9031 9032 9033	20 S10	20 S10
T6029	6017 6018	8 1067^4 8 1068^3	8 1069^2 8 1070^1	T6018d	6015 6016	2 1063$_4$ 8 1061$_3$	2 1063$_2$ 8 1062$_1$
T6032	6019 6020	2 1071 8 1067a^4 8 1068a^3	2 1071 8 1069a^2 8 1070a^1	T9029d	9025 9026 9027	8 1057^4 8 1058^3	8 1059^2 8 1060^1
T9025	9001 9002 9003	7 1009^4 7 1010^3	7 1011^2 7 1012^1	T6018m	6013 6014	2 1054$_4$ 8 1048$_3$	2 1054$_2$ 8 1049$_1$
T9029	9004 9005 9006	8 1013^4 8 1014^3	8 1015^2 8 1016^1	T9029m	9022 9023 9024	8 1050^4 8 1051^3	8 1052^2 8 1053^1

The steel for the main tensile reinforcement was hot-rolled, deformed bars of Swedish fabrication (SKS 52, SKS 60, and SKS 90). Two bars of length 12 m were used for each of the beams T 52 and T 60. The steel SKS 90 was available in lengths of 10 m only, hence three bars were used for each beam T 90. The bars were labelled 5201, 5202, ..., 6001, 6002, ..., and 9001, 9002, ... , respectively. The top reinforcement consisted of two bars SKS 42 of diameter 12 mm. As flange reinforcement and as stirrups in the anchorage zones and in the bending span were used smooth, mild steel of diameter 8 mm.

Most beams had shear reinforcement of mild steel (St. 37) in smooth bars of diameters 6 mm (R6) and 10 mm (R10). Four beams had stirrups of cold-drawn Swedish steel (Ss50) in smooth bars of diameter 10 mm (S 10).

The 6 mm mild steel was delivered in bars of 10 m, which were cut into seven stirrups and a test specimen. Each bar was given an identification number 601, 602, ... etc. The same number designates each of the seven stirrups taken from the particular bar.

The 10 mm mild steel came in bars of length 12 m, which yielded eight stirrups plus a test specimen. The bars (stirrups) were numbered 1001, 1002, ... etc.

The 10 mm cold-drawn steel was delivered in rolls. The stirrups and test specimens were cut from the same roll, hence no identification numbers were needed.

The main reinforcing bars and stirrups were distributed among the 26 beams as indicated in Table 3.1.1. Corresponding to each beam are listed the identification numbers of main reinforcement and stirrups and the amount of stirrups with each particular number. With the exception of Beam No.T6005 the stirrups were placed in pairs and the numbers were mixed over the shear span. In the case that a shear span contains less than three stirrups with the same number, then the stirrups in question are placed at the ends of the shear span, i.e. closest to the support or to the load.

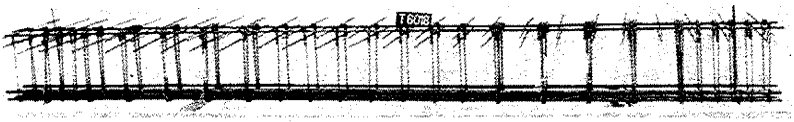

Figure 3.1.1: Completed reinforcement for Beam No.T6018

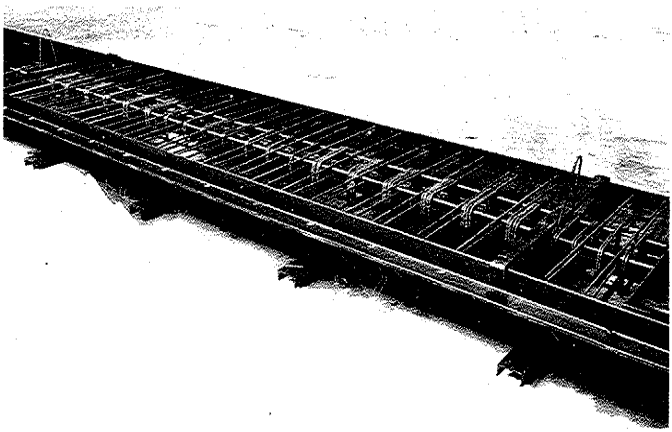

Figure 3.1.2: Beam reinforcement placed in steel mould, ready for casting.

Two stirrups of each shear span were equipped with electrical resistance strain gauges, two companion gauges in the middle of one leg, i.e. a total of eight gauges per beam. The stirrup gauges are indicated in Table 3.1.1 by the small numbers 1,2,3, and 4 (cf. Figure 3.5.1).

After completion of the beam reinforcement, a photograph was taken, a typical example being shown on Figure 3.1.1. Note the electrical resistance strain gauges on four stirrups.

The beams were cast in steel moulds (Figure 3.1.2) together with 9 or 10 companion cylinders.

Three batches of concrete were used for each beam, the recipe for each batch being as follows:

Water	:	34.4 l
Cement	:	27-28 kg
Gravel	:	193 kg
Stone	:	194 kg

The cylinders were filled 1/3 from each batch. The cement was portland cement type 'rapid'. The aggregates were sea material. Typical grading curves for gravel (0-8 mm) and stone (8-32 mm) are shown on Figure 3.1.3.

The highly variable (3-7%) water content of the gravel proved to be a serious problem. Immediately before casting, the water content was determined (by evaporation) for three samples, and the average was used to calculate the reduction of water input and the corresponding increase of gravel supply. If necessary, the water admission to the second and third batch was adjusted in order to keep a constant workability of the mix. In spite of all precautions, the concrete quality shows undesirable fluctuations (cf. Section 3.2). Similar strength variations must be expected from batch to batch, implying that the strength of the web concrete is not determined with a satisfactory accuracy.

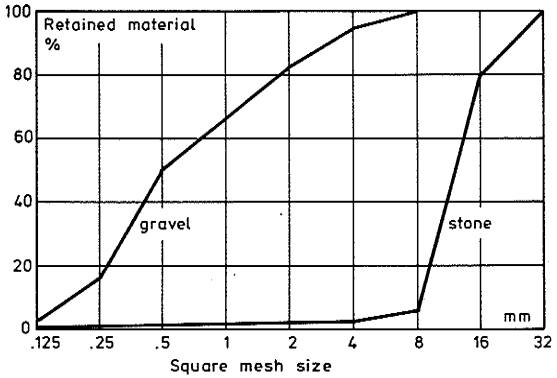

Figure 3.1.3: Grading curves for fine and coarse aggregate

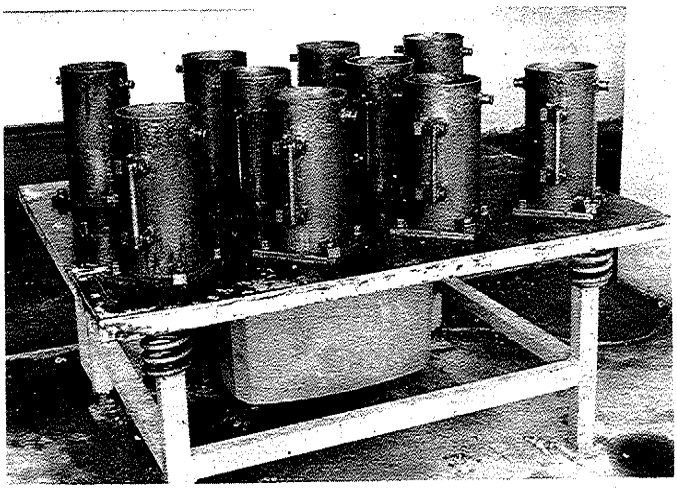

Figure 3.1.4: Cylinder moulds placed on vibrating table

The concrete of the beam was compacted by compressed air vibrators, whereas the cylinder moulds were fixed to a vibrating table, shown on Figure 3.1.4. Beams and cylinders were cured together during four days under wet burlap sacks at a temperature of approximately 20°C. The moulds were stripped two days after casting. Testing took place after 15 days.

3.2 Testing of concrete

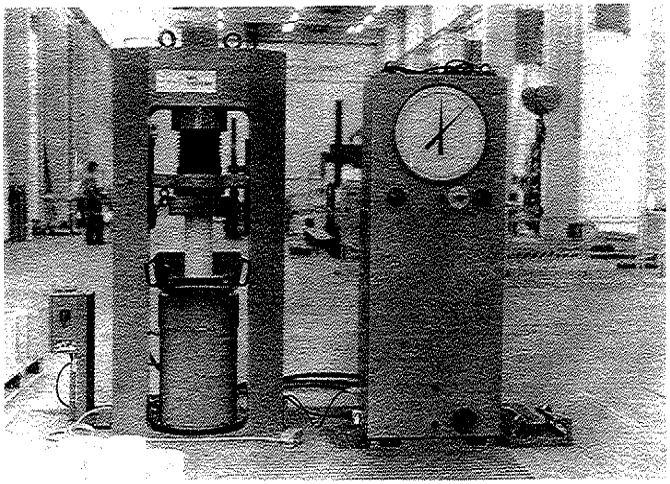

Figure 3.2.1: Concrete cylinder test equipment

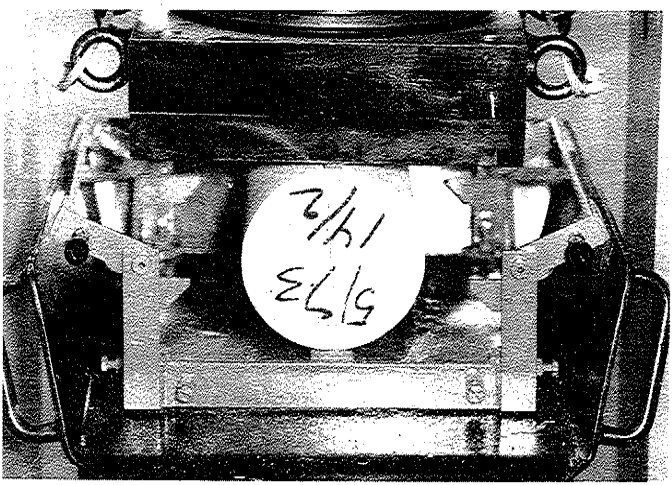

Figure 3.2.2: Close-up view of split cylinder test

The concrete cylinders of height 300 mm and diameter 150 mm were tested in a 200 Mp compression test machine, shown on Figure 3.2.1. Slabs of 10 mm soft fibre board were placed between the specimen and the test machine. Usually the cylinders were tested in the morning and the beam in the afternoon.

The compressive cylinder strength σ_c was determined for five test cylinders per beam. The rate of loading corresponded to approximately 15 kp/cm^2 per minute.

The tensile strength was determined by split cylinder tests on four or five cylinders per beam. The test rig is seen on Figure 3.2.1, below right, and shown in detail on Figure 3.2.2.

Beam Number	Compression tests			Tension tests		
	N	σ_c (kp/cm^2)	s (kp/cm^2)	N	σ_t (kp/cm)	s (kp/cm^2)
T5214	5	109.3	5.46	4	16.60	0.952
T5218	5	105.2	3.14	5	12.29	1.066
T5222	5	104.6	4.86	5	9.65	1.277
T6005	5	107.9	3.86	4	14.60	0.532
T6010	5	105.0	4.36	4	13.20	1.088
T6014	4	115.9	2.32	4	14.96	1.296
T6018	5	112.0	4.04	4	13.15	0.671
T6022	5	105.5	4.25	4	15.01	1.193
T6025	5	104.5	1.67	5	11.30	0.998
T6029	5	107.6	4.36	5	11.94	1.762
T6032	5	119.8	3.46	5	12.39	1.895
T9025	5	127.9	3.62	5	13.44	1.350
T9029	5	81.1	5.78	5	9.80	0.742
T9032	5	100.6	6.69	5	11.46	1.073
T9036	5	107.3	6.78	5	11.50	0.972
T9040	5	114.8	5.71	5	10.50	1.504
T9043	5	105.2	1.77	5	10.62	1.297
T9047	5	128.5	9.90	5	14.05	1.489
T9060	5	121.3	2.30	4	12.12	0.408
T9065	5	102.4	3.16	4	11.19	0.798
T9071	5	111.3	1.92	5	12.43	1.399
T9078	5	114.7	1.59	5	12.26	0.660
T6018d	5	98.1	3.09	5	10.24	1.290
T9029d	5	109.9	4.44	5	12.04	1.476
T6018m	5	106.8	2.37	4	12.85	0.353
T9029m	5	116.2	3.68	5	12.79	2.408

Table 3.2.1: Concrete test results

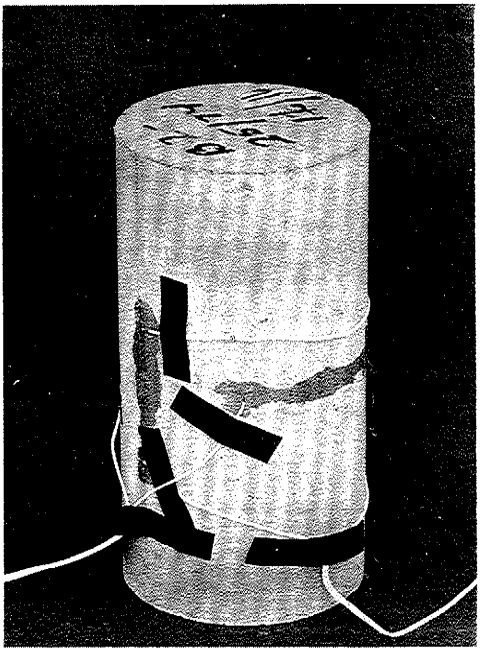

Figure 3.2.3: Test cylinder with electrical resistance strain gauges

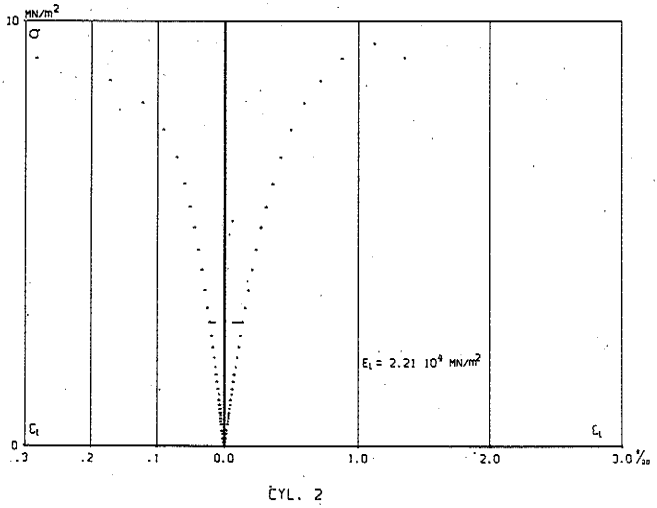

Figure 3.2.4: Longitudinal and transverse strain curves from compressive concrete cylinder test.

The load was applied on a strip of width 15 mm and the split cylinder strength σ_t is defined as:

$$\sigma_t = \frac{2P}{\pi HD}$$

Here P is the ultimate load, H and D being height and diameter of the cylinder, respectively. The rate of loading corresponded to approximately 4 kp/cm^2 per minute.

As discussed in reference [7], it is doubtful whether the split cylinder strength is very representative of the true uniaxial strength of the concrete. At any rate, the tensile strength is not used in the present analysis, the tests being carried out merely for the record.

The failure loads, read from the manometer, were punched on cards and analysed in subroutine CONCR of the computer programme described in Section 4.1. The results are summarized in Table 3.2.1. Corresponding to each beam, the table lists the number N of test cylinders, the average strength σ_c or σ_t, and the standard deviation s .

Four compressive test cylinders corresponding to Beam No. T6018d, were equipped with electrical resistance strain gauges, as shown on Figure 3.2.3. The load and the gauges recording longitudinal and transverse strain were scanned every 10 seconds during the test. The readings were punched on a paper-tape, which was converted to punched cards and analyzed by the computer programme CONC, described in Section 4.1. The output includes a plot of the longitudinal strain ε_l and transverse strain ε_t against concrete stress σ . A typical example is shown on Figure 3.2.4. The horizontal line indicates the proportionality limit. As the test is load-governed, no importance should be attached to the falling branch of the stress -strain curve.

The results from the four cylinders are listed in Table 3.2.2. The programme calculates the elastic modulus E_l of longidudinal strain, the elastic modulus E_t of transverse strain, and Poisson's ratio, defined as E_l/E_t. The failure strain ε_F

Cylinder No.	1	2	3	4/1	4/2
E_l (Mp/cm^2)	243	225	206	160	213
E_l/E_t	0.143	0.162	0.180	0.114	0.164
ε_F (%)	1.3	1.1	1.4	1.9	1.2

Table 3.2.2: Results of loading tests on concrete cylinders

is read on the plots as the longitudinal strain corresponding to maximum stress.

The test (4/1) of Cylinder No.4 was stopped immediately after the load started dropping. The cylinder was then reloaded (4/2) to failure once more, the second failure load being the same as the first.

In Table 3.2.2, it is noted that the observed failure strains are rather small. A value $\varepsilon_F = 2.0\%$ is considered normal.

3.3 Testing of stirrup reinforcement

A test specimen was taken in the middle of each of the mild steel bars, amounting to a total of 20 specimens R6 and 75 specimens R10. From the cold-drawn reinforcement S10, 20 test specimens were taken in different places of the roll.

The specimens were tested in a MOHR-FEDERHAFF 60 Mp tension test machine, shown on Figure 3.3.1. The rate of loading up to yield was approximately 20 kp/sec, 50 kp/sec, and 50 kp/sec for R6, R10, and S10, respectively. The yield strength P_Y and the ultimate strength P_u were recorded visually from the manometer. The strain was measured over an interval of 100 mm by an extensometer clamped onto the bar, as seen on Figure 3.3.2. A load-strain curve was drawn automatically, the load being measured by an oil pressure cell. Typical curves for mild and cold-drawn steel are shown on Figures 3.3.3a and b, respectively. The figures also show the idealized force-strain curve used in the analysis. On the graphs, the force-strain modulus E_s is measured and the yield strain controlled. The ultimate strain ε_u was measured for a few of the specimens by means of marks placed on the bar at 10 mm intervals prior to testing.

The test results are summarized in Tables 3.3.1a, b, and c. The yield strength P_Y for the mild steel reinforcement R6 and R10 is the load at which yielding is registered on the manometer. For the cold-drawn steel S10, no definite yield point could be detected, hence P_Y is defined as the 2‰ offset strength measured on the force-strain graph.

A few of the results for the reinforcement R10 are lacking, because the corresponding specimens have been mislaid. In such cases, the average values of P_Y and E_s are used in the analysis. For the reinforcement S10, the average values are used throughout.

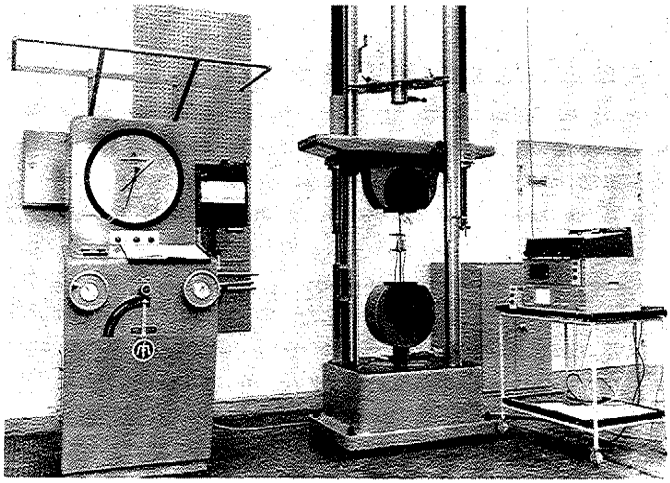

Figure 3.3.1: Tension test of stirrup reinforcement

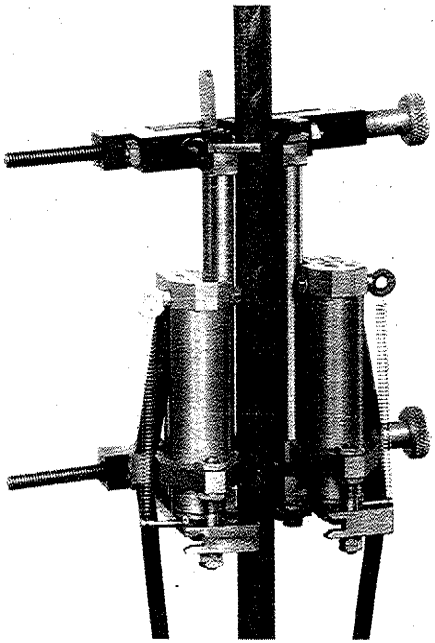

Figure 3.3.2: Extensometer clamped to test specimen

a)

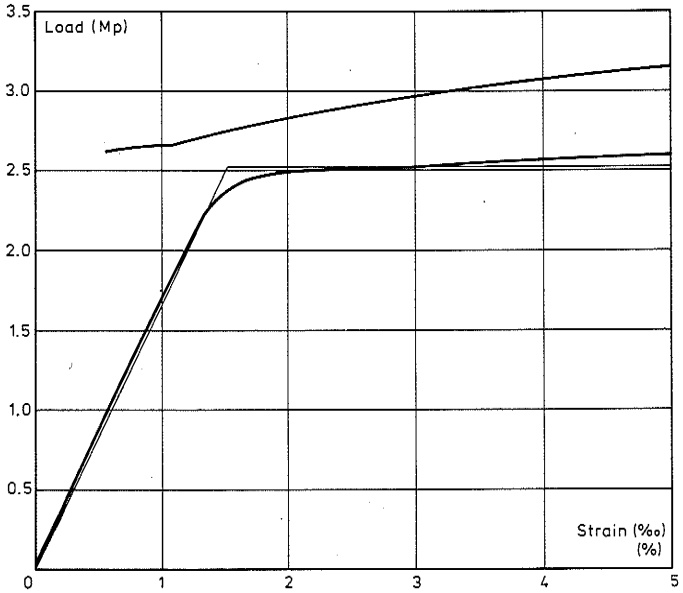

b)

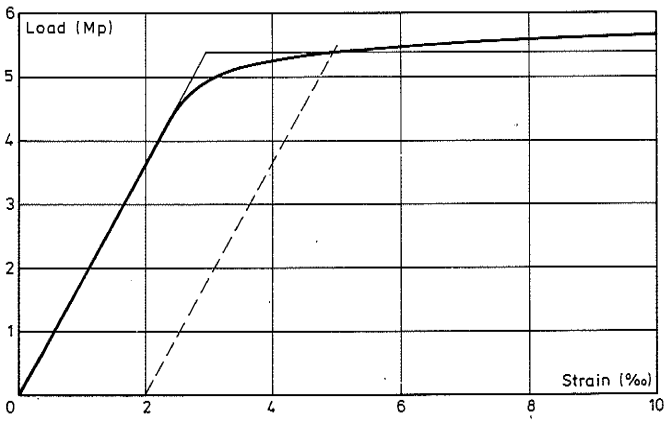

Figure 3.3.3: Actual and idealized load-strain curves for stirrup reinforcement

a) Mild steel (Bar No.1065)
b) Cold-drawn steel (Bar No.2)

a)

Bar No	P_y (kp)	P_u (kp)	E_s (Mp)	ε_u (%)	Bar No	P_y (kp)	P_u (kp)	E_s (Mp)	ε_u (%)
601	930	1200	635	-	611	963	1220	625	17
602	900	1165	630	-	612	902	1152	607	-
603	928	1184	624	-	613	936	1215	625	-
604	936	1240	597	17	614	934	1230	612	-
605	928	1192	609	-	615	930	1193	606	-
606	910	1182	593	-	616	950	1239	625	-
607	934	1200	630	-	617	890	1180	612	-
608	972	1240	582	-	618	936	1205	625	-
609	928	1230	612	-	619	930	1188	648	-
610	976	1220	630	-	620	930	-	594	-
Average						932	1204	616	-
Coefficient of variation (%)						2.3	2.1	2.7	-
Nominal yield stress: 3300 kp/cm^2					Nominal elastic modulus:2.18 Gp/cm^2				

b)

Bar No	P_y (kp)	P_u (kp)	E_s (Mp)	ε_u (%)	Bar No	P_y (kp)	P_u (kp)	E_s (Mp)	ε_u (%)
1001	2700	3200	1620	-	1039	2760	3330	1660	-
1002	2690	3150	1660	12	1040	2400	2940	1600	13
1003	2690	3170	1680	-	1041	2760	3280	1720	-
1004	2400	3025	1700	16	1042	2580	3220	1710	-
1005	2710	3213	1635	-	1043	2560	3230	1680	-
1006	2480	3105	1635	6	1044	2720	3300	1600	-
1007	2760	3240	1620	-	1045	2620	3200	1800	-
1008	2610	3135	1635	11	1046	2610	3250	1650	10
1009	2660	3270	1870	-	1047	2600	3180	1650	-
1010	2650	3180	1590	-	1048	2680	3240	1690	-
1011	2670	3220	1620	-	1049	2200	2920	1600	-
1012	2700	3200	1605	-	1050	2330	2940	1710	-
1013	2700	3330	1635	-	1051	2690	3240	1600	-
1014	2650	3150	1635	-	1052	2790	3330	1600	8
1015	2320	2960	1605	-	1053	-	-	-	-
1016	2660	3150	1635	-	1054	2650	3160	1650	-
1017	2750	3220	1680	-	1055	2310	2930	1600	-
1018	2700	3220	1920	-	1056	2820	3320	1660	-
1019	2795	3250	1650	11	1057	2770	3280	1680	-
1020	2730	3220	1695	-	1058	2340	2930	1640	11
1021	2745	3260	1785	-	1059	2360	2960	1640	-
1022	2725	3190	1720	-	1060	2660	3230	1660	-
1023	2700	3200	1575	-	1061	-	-	-	-
1024	2740	3190	1650	-	1062	2680	2930	1640	10
1025	2350	2980	1650	-	1063	-	-	-	-
1026	2450	2970	1860	-	1064	2560	3190	1600	-
1027	2390	2950	1650	-	1065	2525	3240	1660	-
1028	2190	2885	1710	-	1066	2760	3270	1800	-
1029	2580	3170	1650	-	1067	-	-	-	-
1030	2340	2920	1640	18	1068	-	-	-	-
1031	2650	3220	1620	-	1069	-	-	-	-
1032	2330	2940	1640	-	1070	2650	3400	1620	-
1033	2200	2920	1780	-	1067a	2760	3360	1690	-
1034	2590	3130	1600	-	1068a	2270	2960	1600	-
1035	2720	3260	1650	-	1069a	2340	2920	1660	-
1036	2110	2860	1600	-	1070a	2330	2920	1700	-
1037	2200	2920	1600	-	1071	2510	3170	1640	-
1038	2660	3160	1620	-					
Average						2570	3140	1660	-
Coefficient of variation (%)						7.2	4.6	4.1	-
Nominal yield stress: 3270					Nominal elastic modulus:2.11 Gp/cm^2				

c)

Test No	P_y (kp)	P_u (kp)	E_s (Mp)	ε_u (%)	Test No	P_y (kp)	P_u (kp)	E_s (Mp)	ε_u (%)
1	5300	5660	1760	-	11	5075	5720	1890	-
2	5400	6100	1820	4	12	5125	5770	1820	-
3	5450	6180	1880	-	13	5150	5790	1820	-
4	5175	5780	1920	-	14	5000	5620	1820	-
5	5450	6190	1840	-	15	5000	5610	1850	5
6	5150	5800	1840	-	16	5100	5750	1840	-
7	5100	5770	1890	-	17	5125	5770	1840	-
8	5075	5730	1880	-	18	5025	5660	1840	-
9	5100	5720	1840	4	19	5100	5760	1850	-
10	5425	6180	1840	-	20	5050	5720	1820	-
Average						5170	5815	1845	-
Coefficient of variation (%)						2.9	3.2	1.9	-
Nominal yield stress: 6580 kp/cm^2					Nominal elastic modulus:2.35 Gp/cm^2				

Table 3.3.1: Tension test results for stirrup reinforcement

a) 6 mm mild steel
b) 10 mm mild steel
c) 10 mm cold-drawn steel

In addition to the average values and coefficients of variation, the tables state the nominal yield stress and the nominal elastic modulus, defined as the average values of P_y and E_s, divided by the nominal cross-sectional area.

The average stirrup strength for each shear span is found using the strength data and the distribution of stirrups (Table 3.1.1). The stirrups at the ends of the shear span have been disregarded by the calculation of the average stirrup strength. Introducing the stirrup spacings (Table 2.2.1), the equivalent stirrup strength s_y is computed for each shear span. The results are listed in Table 4.2.1.

CALIBRATION OF ELECTRICAL RESISTANCE STRAIN GAUGES

SCANS						
11.08	500*20	0*20	-1518*51	-1491*51	-1504*51	-1503*51
11.16	500*20	101*20	-1338*51	-1329*51	-1319*51	-1353*51
11.17	501*20	200*20	-1159*51	-1189*51	-1189*51	-1162*51
11.18	500*20	302*20	-973*51	-1036*51	-1048*51	-961*51
11.20	500*20	400*20	-795*51	-892*51	-915*51	-775*51
11.21	500*20	497*20	-558*51	-788*51	-849*51	-474*51
11.22	500*20	557*20	167*51	-782*51	-828*51	211*51
11.22	500*20	559*20	201*51	-777*51	-812*51	223*51
11.23	500*20	598*20	600*51	600*51	600*51	600*51

GAUGE STRAINS (0/00)

TIME	LOAD (KP)	GAUGE 1	GAUGE 2	GAUGE 3	GAUGE 4	AVERAGE
11.08	0.	0.00	0.00	0.00	0.00	0.00
11.16	495.	0.31	0.28	0.32	0.26	0.30
11.17	980.	0.62	0.53	0.53	0.59	0.57
11.18	1480.	0.95	0.79	0.80	0.95	0.87
11.20	1964.	1.26	1.05	1.03	1.27	1.15
11.21	2455.	1.68	1.23	1.15	1.60	1.46
11.22	2729.	2.94	1.24	1.18	2.99	2.09
11.22	2730.	3.09	1.25	1.21	3.01	2.12
11.23	2930.	*****	*****	*****	*****	*****

Table 3.3.2: Results from strain gauges on stirrup specimen

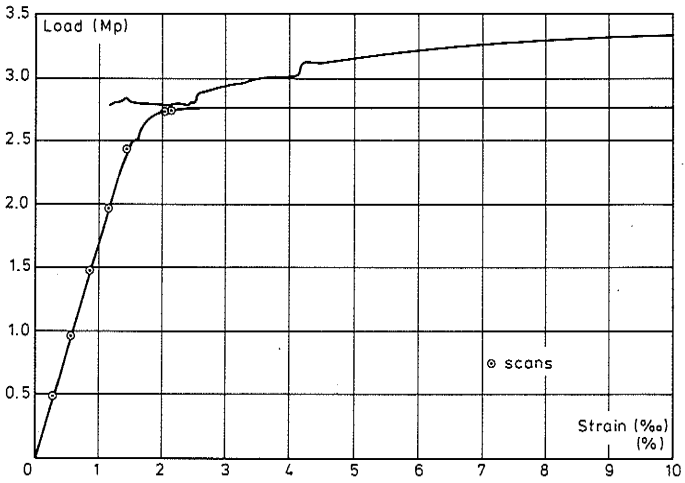

Figure 3.3.4: Strain measurements by extensometer and by electrical resistance strain gauges (Bar No.1067a)

In order to check the strain measurement on the stirrups in the beam (cf. Sections 3.5 and 4.5) a test specimen (from Bar No.1067a) was equipped with four electrical resistance strain gauges in addition to the extensometer. The strain gauge readings were analyzed by the computer programme GAUGE (cf. Section 4.1), the output being shown in Table 3.3.2. On figure 3.3.4 the strain gauge scans are plotted on the force-strain graph taken from the extensometer. The agreement of the strain measurements is excellent. The load signals are supplied by the same pressure cell.

3.4 Testing of longitudinal reinforcement

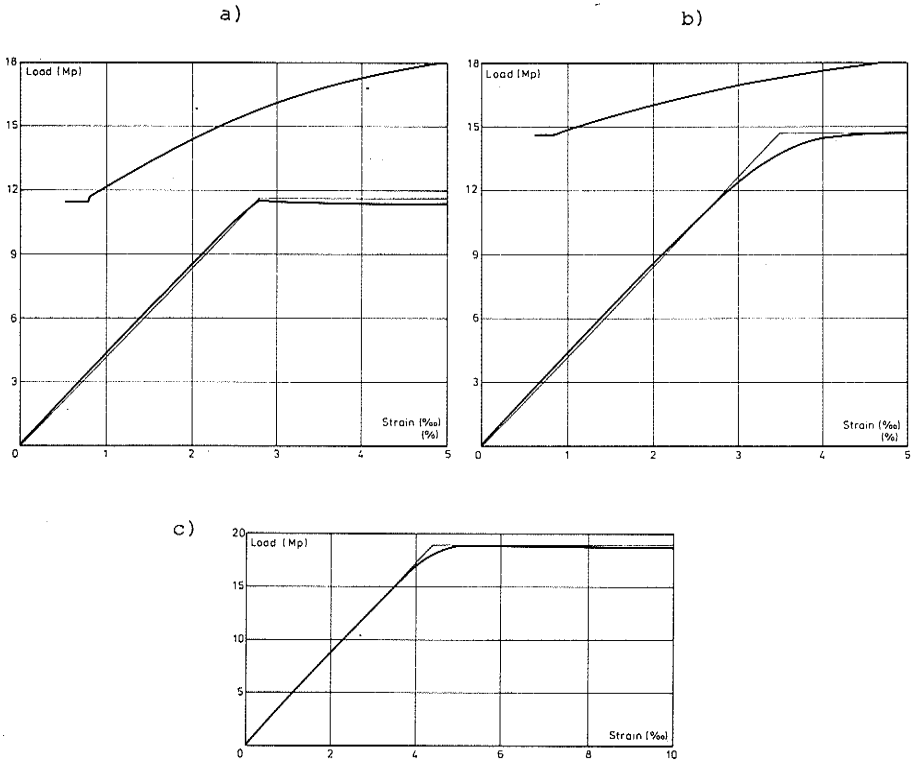

Figure 3.4.1: Actual and idealized load-strain curves for main reinforcement

a) Steel SKS 52 (Bar No.5206)
b) Steel SKS 60 (Bar No.6020)
c) Steel SKS 90 (Bar No.9019)

A tensile test specimen was taken in the interior of each bar of main reinforcement, totalling 6 specimens SKS52, 20 specimens SKS 60, and 39 specimens SKS 90. In order to control the yield strength, a few of the bars were tested at the start of the programme. As the strength turned out to be fairly constant, and because the properties of the main reinforcement is relatively unimportant for the shear analysis, it was decided mainly to test the specimens corresponding to the beams which got or almost got flexural failure (cf. Section 4.2). Consequently, only 10 specimens SKS 60 and 18 specimens SKS 90 were tested.

The test equipment and procedure is identical with the one described in the preceding section for the shear reinforcement, except for the rate of loading, which was approximately 200 kp/sec. Typical force-strain curves are shown on Figure 3.4.1, together with the idealized curves used in the flexural analysis.

The three curves are strikingly similar. The rather sharp yield point on Figure 3.4.1a appears because yielding has started outside the 100 mm range of the extensometer. The sudden jump in load at a strain of 0.8% on the same figure, corresponds to an increase in the rate of loading.

The results of the tests are summarized in Tables 3.4.1a,b, and c. For the bars not tested the average values are used.

The top reinforcement was not tested systematically, but a few specimens were taken at random, to give an idea of the strength. Table 3.4.2 contains the results, and the average values are used in the analysis.

The test data from the longitudinal reinforcement and the concrete strengths are used in the flexural analysis of the beams (cf. Section 2.3). The flexural failure loads are also given in Table 4.2.1 of the following chapter.

a)

Bar No.	P_Y (Mp)	P_u (Mp)	E_s (Gp)	ε_u %	Bar No.	P_Y (Mp)	P_u (Mp)	E_s (Gp)	ε_u (%)
5201	11.6	19.3	4.35	-	5204	11.45	18.7	4.1	-
5202	11.5	19.1	4.15	15	5205	11.6	19.2	4.15	-
5203	11.15	18.6	4.1	-	5206	11.6	19.2	4.15	12
Average						11.5	19.0	4.15	-
Coefficient of variation (%)						1.5	1.5	2.2	-
Nominal yield stress: 5700 kp/cm^2					Nominal elastic mudulus: 2.06 Gp/cm^2				

b)

Bar No.	P_Y (Mp)	P_u (Mp)	E_s (Gp)	ε_u %	Bar No.	P_Y (Mp)	P_u (Mp)	E_s (Gp)	ε_u (%)
6001	14.75	18.0	4.5	-	6006	14.7	17.7	4.35	12
6002	14.75	18.05	4.5	15	6017	14.75	18.5	4.3	-
6003	14.8	-	4.2	-	6018	14.8	18.55	4.3	-
6004	15.0	18.15	4.5	-	6019	14.55	17.5	4.3	-
6005	14.95	18.5	4.2	-	6020	14.7	18.85	4.2	-
Average						14.8	18.2	4.35	-
Coefficient of variation (%)						0.9	2.4	2.9	-
Nominal yield stress: 7400 kp/cm^2					Nominal elastic modulus:2.16 Gp/cm^2				

c)

Bar No.	P_Y (Mp)	P_u (Mp)	E_s (Gp)	ε_u %	Bar No.	P_Y (Mp)	P_u (Mp)	E_s (Gp)	ε_u %
9004	18.95	20.2	4.2	-	9016	18.7	20.2	4.3	-
9005	18.35	20.3	4.2	-	9017	18.2	20.25	4.2	-
9006	18.6	20.05	4.1	-	9018	18.5	20.1	4.3	8
9010	18.15	20.5	4.2	-	9019	18.85	20.35	4.3	-
9011	18.35	20.25	4.2	-	9020	18.85	20.35	4.2	-
9012	18.7	20.1	4.3	5	9021	18.35	20.25	4.3	-
9013	18.6	20.1	4.35	6	9022	17.95	20.3	4.2	-
9014	17.8	20.25	4.2	-	9023	17.75	20.2	4.2	-
9015	18.8	20.1	4.3	-	9024	17.9	20.25	4.3	-
Average						18.4	20.25	4.25	-
Coefficient of variation (%)						2.1	0.6	1.5	-
Nominal yield stress:9150 kp/cm^2 Nominal elastic modulus:2.11 Gp/cm^2									

Table 3.4.1: Tension test results for 16 mm longitudinal bottom reinforcement.

a) Steel quality SKS 52
b) Steel quality SKS 60
c) Steel quality SKS 90

Test No.	P_Y (Mp)	P_u (Mp)	E_s (Gp)	ε_u %	Test No.	P_Y (Mp)	P_u (Mp)	E_s (Gp)	ε_u %
1	5.26	8.81	2.34	-	3	5.43	9.00	2.32	11
2	5.27	8.77	2.34	-	4	4.68	7.15	2.36	-
Average						5.16	8.43	2.34	-
Coefficient of variation (%)						6.4	10.2	0.7	-
Nominal yield stress 4570 kp/cm^2 Nominal elastic modulus:2.07 Gp/cm^2									

Table 3.4.2: Tension test results for 12 mm longitudinal top reinforcement (SKS 42).

3.5 Testing of beams

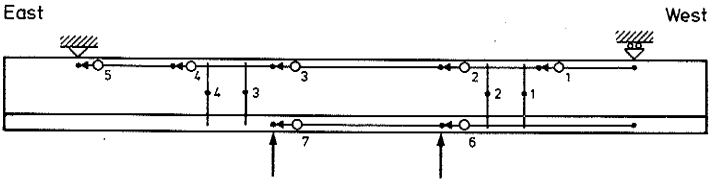

Figure 3.5.1: Loading diagram and positions of gauge stirrups and dial gauges

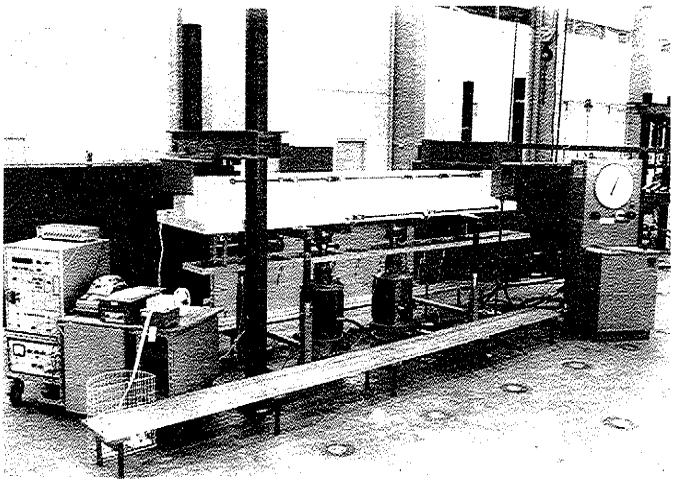

Figure 3.5.2: Overall view of beam test rig

The loading diagram is sketched on Figure 3.5.1, whereas Figure 3.5.2 shows the actual test rig. The beams were tested upside down, the loads being supplied by 100 Mp AMSLER hydraulic jacks. The load was applied over the total width of the flange by means of a cross-beam, shown on Figure 3.5.3. The stiffness of the cross-beam is such that a load of 30 Mp equally distributed over the cross-beam would cause a maximum deflexion of 1 mm. At loading, a 10 mm soft fibre board was placed between the cross-beam and the flange.

The supports were rocker bearings, consisting of 50 mm diameter cylinders fitting into grooves in 40 mm × 150 mm × 300 mm steel platens (cf. Figure 3.5.4). The grooves were circular of width 60 mm and depth 9 mm, the radius being 55 mm. A slab of 4 mm hard fibre board was placed between the platen and the web. The moveable (western) support, shown on Figure 3.5.4, was built as a 3 m radius pendulum bearing.

The load on the jacks was measured by an AMSLER spring manometer with pressostate (seen to the right on Figure 3.5.2). The magnitude was read visually on the scale of the manometer and recorded electrically by a device connected to the scale hand. Electrical resistance transducers shown on Figure 3.5.3 recorded the deflexions of the flange at 300 mm intervals. The strains in two stirrups in the middle of each shear span were measured by electrical resistance strain gauges, two opposite each others in the middle of each stirrup. The positions of the gauge stirrups is shown on Figure 3.5.1.

All the electrical measurements were registered automatically on a solartron, placed to the left on Figure 3.5.2. In addition to the time, each scan covered 20 channels, viz.:

- The voltage of the Wheatstone's bridge
- The load at the start of the scan.
- Eight stirrup strain readings.
- Nine deflexion readings.
- The load at the end of the scan.

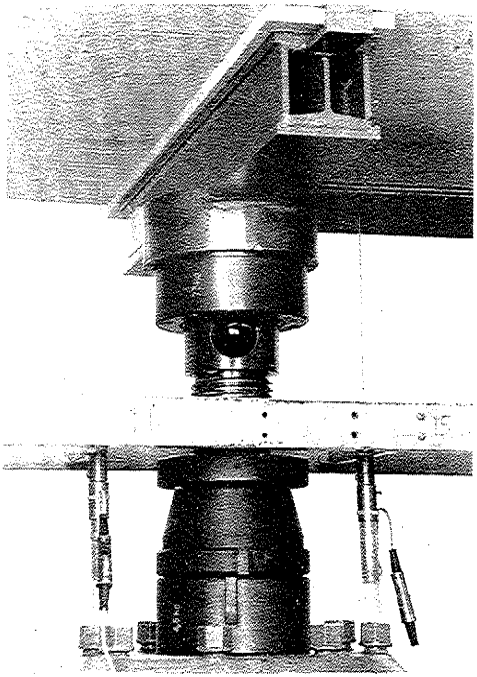

Figure 3.5.3: Jack head with cross-beam. Resistance transducers for deflexion measurements.

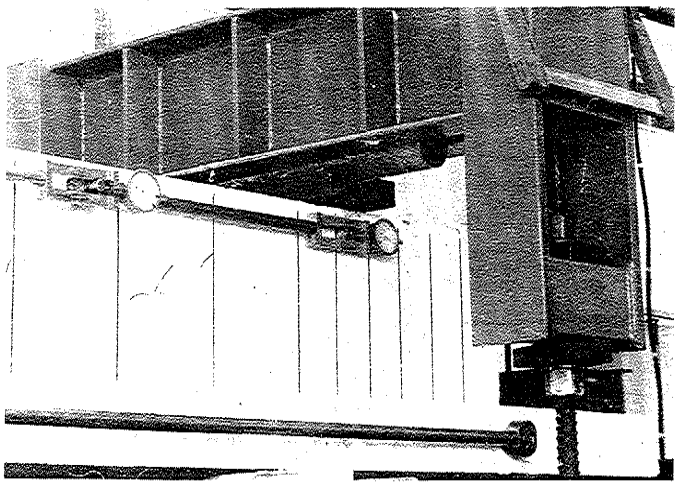

Figure 3.5.4: Western beam end with pendulum support and dial gauges on the beam faces.

Each scan took approximately 40 seconds, and the readings were punched on a papertape and printed for visual inspection. The papertape was later converted to punched cards.

Longitudinal strain measurements were taken by means of 7 dial gauges on each side of the beam. The position of the gauges is sketched on Figure 3.5.1 and details are seen on Figure 3.5.4. The bearings for the dial gauges were screwed into nuts placed in the beam mould prior to casting. Gauges 1 through 5 measure the elongations at the level of the main reinforcement. Gauges 6 and 7 are placed in the central level of the flange and record the flange compression in the shear and bending span, respectively. Because of the test rig, it was only feasible to measure the compression of the western shear span flange. The dial gauge readings were recorded visually and the values were later punched on cards.

A zero measurement was taken with the beam resting on the jacks. The beam was then loaded in steps of 2 Mp (per jack), apart from the first two steps of 3 Mp each. Up to 10 Mp, the load was applied during 5 minutes, including 1 minute for the actual loading. Then the dial gauges were read and at least two scans taken at a total duration of 2 minutes. At loads of 10 Mp and more, the load was applied during 10 minutes before the measurements. When the beam was near failure, i.e. when considerable deformations were taking place at constant load, measurements were taken at 5 minutes interval. A typical loading history is shown in Section 4.3.

The shear cracking load, and the load at which the shear cracks extended into the flange, and the ultimate load were noted. On the whitewashed beam, the cracks were traced with ink and photographed at load intervals of 4 Mp, starting at 10 Mp. After failure, the dial gauges and deflexion transducers were removed and an additional photograph was taken.

When one of the shear spans had failed, the corresponding hydraulic jack was closed down, and loading proceded until failure of the other shear span. The shear force in the span is now 195/300 P, P being the load on the jack. Therefore the

load steps are increased by a factor 300/195 = 1.54. The load was raised at intervals of 7 minutes, but for the greater part of the second test, the loading was not well controlled, since it was found that the other hydraulic jack continued to exert a force on the beam after the oil supply had been cut off. Prior to failure of the span, however, it was assured that only the loaded jack was touching the beam.

At the second test, only the stirrup strains were recorded at each load step, and the ultimate load was noted. In some cases, a second shear failure was not achieved, either because the manipulation of the jacks did not succeed, or because the beam failed in the same end as before.

After completion of the test, close-up photographs were taken of the failure(s) on the opposite side of the beam, where the cracks had not been traced.

4. TEST ANALYSIS

4.1 Computer programmes

The data from the beam tests were analysed by the computer programme PLOT, which was written in FORTRAN and run on the IBM 370/165 computer facilities of NEUCC at the Technical University of Denmark. Figure 4.1.1 shows the structure of the computer programme. The analysis is carried out in eight subroutines, operating as follows:

Subroutine HEAD prints the first page of the output, identifying the beam and listing the dates of casting and testing, the material properties and the ultimate load or loads. A typical example is shown as Figure 4.1.2. The first page also contains the analysis of the concrete test results (cf.Section 3.2), which is performed in the subroutine CONCR. Subroutine SCAN converts the content of the papertape to readings in volts. The actual numbers recorded during the test are printed as page two of the output (Table 4.1.1). Subroutine LOADS calculates the loads and plots the loading history (cf. Section 4.3). Subroutine DEFLEX calculates and prints the deflexions and plots deflexion curves (cf. Section 4.3). Subroutine DIALS analyses the dial gauge readings (cf. Section 4.4). Subroutine GAUGES analyses the stirrup strain readings (cf. Section 4.5). Subroutine FORCES calculates, prints, and plots the forces in the four stirrups equipped with strain gauges (cf.Section 4.5).

The five subroutines ASTEX, RECTAN, TEXT, GRAPHS, and LEGEND perform routine operations common to several of the subprogrammes mentioned above.

Another programme, RELOAD, combining parts of subroutines SCAN, LOADS, and GAUGES, was used to treat the strain measurements of the second beam test (cf. Section 4.6). In this case, no plots were made. The calibration of the strain gauges, described in Section 3.3, was carried out using a similar programme, GAUGE.

The strain data from the concrete cylinder loading tests,

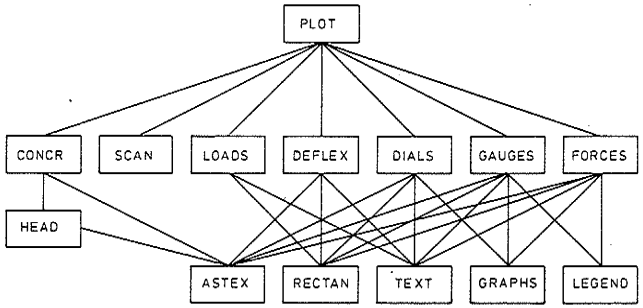

Figure 4.4.1: Structure of computer programme for analysis of data from beam tests

```
S H E A R   S T R E N G T H   O F   R E I N F O R C E D   C O N C R E T E   B E A M S

STRUCTURAL RESEARCH LABORATORY
STVF        2549. B-257
DATE:       1975. 9.11

**********************************************************************************************************************

BEAM NO:  T6018                    CAST:  1973.10.23                    TESTED:  1973.11.07
CONCRETE STRENGTH:                 SIGMAC:   112.  KP/SQCM              STIRRUPS:  2R10/210.0 MM
SHEAR REINFORCEMENT EAST:          SIGMAY:  3431.  KP/SQCM                   PSI:  0.229
SHEAR REINFORCEMENT WEST:          SIGMAY:  3240.  KP/SQCM                   PSI:  0.216
SHEAR FAILURE LOAD WEST:              PU:    24.5 MP                  TAU/SIGMAC:  0.348
SHEAR FAILURE LOAD EAST:              PU:    23.5 MP                  TAU/SIGMAC:  0.334

**********************************************************************************************************************

CONCRETE STRENGTHS:

CYLINDER STRENGTHS       (KP/SQCM):      114.8    113.6    112.4    104.9    114.2
SPLIT CYLINDER STRENGTHS (KP/SQCM):       12.5     12.8     13.4     14.0


AVERAGE CYLINDER STRENGTH:          112.0  KP/SQCM      AVERAGE SPLIT CYLINDER STRENGTH:     13.15  KP/SQCM
STANDARD DEVIATION:                   4.04 KP/SQCM      STANDARD DEVIATION:                   0.671 KP/SQCM

**********************************************************************************************************************
```

Figure 4.1.2: First page of output from Beam No.T6018

described in Section 3.2, were analysed by CONC, adapted from a standard programme developed at the Structural Research Laboratory. Based upon the experimental stress-strain curve, the elastic modulus is calculated as follows: By the method of least squares, a straight line is constructed through the first (standard: 8) points of the curve. The next point is included if it lies close enough (standard: strain difference less than 0.007%) to the line. If the point is included, a new line is calculated, and the process is repeated until the stress-strain curve deviates too much from the line. When the results are plotted (see Section 3.2), the strain values are adjusted in order to let the line pass through the origin.

Table 4.1.1: Numbers recorded during scans of Beam No.T6018

RECORDING OF ALL SCANS

12:48 500*20	1*20	-1526*51 -596*22	-1527*51 -470*22	-1522*51 -504*22	-1523*51 -197*22	-1522*51 -301*22	-1525*51 -217*22	-1479*51 -429*22	-1520*51 -384*22	-372*22	2*20
12:56 500*20	62*20	-1524*51 -587*22	-1527*51 -450*22	-1516*51 -475*22	-1521*51 -165*22	-1523*51 -264*22	-1531*51 -177*22	-1478*51 -400*22	-1517*51 -363*22	-360*22	62*20
13:05 500*20	122*20	-1444*51 -564*22	-1475*51 -409*22	-1473*51 -418*22	-1483*51 -95*22	-1465*51 -192*22	-1430*51 -100*22	-1454*51 -342*22	-1476*51 -324*22	-336*22	122*20
13:12 500*20	163*20	-1330*51 -548*22	-1391*51 -378*22	-1430*51 -371*22	-1438*51 -43*22	-1331*51 -137*22	-1304*51 -54*22	-1419*51 -300*22	-1434*51 -294*22	-321*22	163*20
13:24 500*20	203*20	-1261*51 -529*22	-1319*51 -341*22	-1390*51 -321*22	-1400*51 16*22	-1261*51 -79*22	-1221*51 4*22	-1388*51 -250*22	-1400*51 -261*22	-301*22	203*20
13:36 500*20	244*20	-1190*51 -510*22	-1266*51 -308*22	-1342*51 -266*22	-1330*51 81*22	-1200*51 -8*22	-1150*51 69*22	-1331*51 -197*22	-1339*51 -222*22	-287*22	244*20
13:48 500*20	281*20	-1144*51 -492*22	-1230*51 -270*22	-1279*51 -210*22	-1255*51 149*22	-1144*51 60*22	-1099*51 137*22	-1260*51 -143*22	-1261*51 -184*22	-267*22	281*20
14:00 500*20	321*20	-1078*51 -471*22	-1174*51 -223*22	-1182*51 -137*22	-1139*51 232*22	-1073*51 147*22	-1042*51 218*22	-1180*51 -72*22	-1173*51 -136*22	-248*22	321*20
14:12 500*20	362*20	-988*51 -447*22	-1086*51 -167*22	-1084*51 -54*22	-1012*51 332*22	-981*51 251*22	-976*51 321*22	-1087*51 13*22	-1070*51 -85*22	-226*22	362*20
14:24 500*20	402*20	-874*51 -417*22	-976*51 -102*22	-1020*51 46*22	-887*51 453*22	-870*51 377*22	-925*51 445*22	-918*51 116*22	-942*51 -18*22	-199*22	402*20
14:33 500*20	422*20	-827*51 -402*22	-922*51 -69*22	-985*51 98*22	-828*51 515*22	-812*51 442*22	-900*51 509*22	-839*51 172*22	-897*51 14*22	-183*22	421*20
14:36 500*20	421*20	-828*51 -400*22	-914*51 -63*22	-982*51 108*22	-824*51 525*22	-805*51 454*22	-902*51 520*22	-826*51 183*22	-892*51 20*22	-182*22	421*20
14:48 500*20	442*20	-777*51 -380*22	-836*51 -21*22	-930*51 172*22	-758*51 601*22	-740*51 535*22	-882*51 601*22	-742*51 251*22	-843*51 62*22	-166*22	442*20
14:53 500*20	442*20	-774*51 -379*22	-824*51 -12*22	-933*51 185*22	-751*51 617*22	-731*51 550*22	-886*51 615*22	-730*51 263*22	-837*51 70*22	-162*22	442*20
14:58 500*20	442*20	-763*51 -375*22	-817*51 -8*22	-927*51 194*22	-748*51 628*22	-725*51 560*22	-889*51 628*22	-726*51 273*22	-831*51 76*22	-162*22	442*20
15:03 500*20	442*20	-765*51 -374*22	-810*51 -4*22	-923*51 200*22	-745*51 636*22	-720*51 569*22	-891*51 637*22	-720*51 282*22	-828*51 82*22	-161*22	442*20
15:08 500*20	442*20	-765*51 -373*22	-803*51 2*22	-919*51 206*22	-743*51 643*22	-716*51 578*22	-893*51 644*22	-721*51 287*22	-820*51 85*22	-157*22	442*20
15:13 500*20	442*20	-765*51 -371*22	-799*51 5*22	-917*51 210*22	-743*51 648*22	-713*51 583*22	-895*51 648*22	-721*51 291*22	-815*51 89*22	-156*22	442*20
15:25 500*20	462*20	-698*51 -353*22	-714*51 42*22	-864*51 270*22	-684*51 697*22	-664*51 664*22	-878*51 696*22	-662*51 364*22	-761*51 133*22	-144*22	461*20

The programme FLEX calculates the flexural capacities of the beams, based upon the strengths of concrete and longitudinal reinforcement, found in Chapter 3. The analysis is explained in Section 2.3. If the reinforcement is not yielding, the flexural strength is found by iteration. In Section 2.3, the results are given.

Finally, the programme EXP compares the experimentally obtained ultimate loads with the predictions of the web crushing criterion (cf. Section 1.1). The programme calculates the best value of the web effectiveness ν by minimizing the sum of squares of the normal distances of the experimental points $(\psi, \tau/\sigma_c)$ from the web crushing criterion, equations (2). The output includes the coefficient of variation based upon N-1 degrees of freedom, N being the number of points. The results are stated in Section 4.7.

As mentioned in the introduction, the actual programmes and the entire output is not included in the present report. A general description of the results is given in the sections below.

4.2 General behaviour

The strength properties of the 26 beams are listed in Table 4.2.1. The table contains the material strengths s_y and σ_c (cf. Section 3.3 and 3.2, respectively), the expected flexural failure load P_F (cf. Section 2.3), the observed shear cracking load V_{cr}, the observed ultimate load V_u, and the type of failure. The latter is designated as follows: SE: shear failure of eastern span, SW: shear failure of western span, FT: flexural tension failure, and FC: flexural compression failure. Beam No.T6005 failed in both shear spans simultaneously.

Beam No		s_y (kp/cm²)	σ_c (kp/cm²)	P_F (Mp)	V_c (Mp)	V_u (Mp)	Failure Mode	Beam No.		s_y (kp/cm²)	σ_c (kp/cm²)	P_F (Mp)	V_c (Mp)	V_u (Mp)	Failure Mode
T5214	W	19.4	109	21.6	6	21.9	SW	T9032	W	46.6	101	27.0	6	-	SE
	E	19.3				-			E	47.3				26.3	
T5218	W	24.4	105	21.0	6	22.4	SE	T9036	W	51.8	107	28.3	6	28.6	SW
	E	25.4				21.7			E	52.1				-	
T5222	W	28.9	105	21.5	6	21.2	FT	T9040	W	49.5	115	30.0	8	26.5	SE
	E	29.3							E	52.0				25.4	
T6005	W	6.9	108	26.7	6	16.1	SEW	T9043	W	55.2	105	27.9	6	28.6	SE
	E	7.1				16.1			E	56.7				27.6	
T6010	W	14.1	105	26.7	6	-	SE	T9047	W	62.3	129	32.9	6 ?	28.6	SW
	E	14.2				19.4			E	59.9				30.4	
T6014	W	19.5	116	26.9	6	24.2	SE	T9060	W	68.9	121	31.2	8 ?	24.5	SW
	E	19.9				22.7			E					24.3	
T6018	W	24.2	112	26.8	8	24.5	SW	T9065	W	78.9	102	27.2	8	24.5	SE
	E	25.7				23.5			E					24.5	
T6022	W	30.7	106	26.6	8 ?	23.9	SE	T9071	W	88.4	111	29.1	8	26.5	SE
	E	29.7				22.4			E					24.5	
T6025	W	34.7	105	26.6	6	22.4	SW	T9078	W	98.5	115	30.0	10	28.6	SE
	E	35.6				24.2			E					26.5	
T6029	W	39.8	108	26.7	6	26.5	SE	T6018d	W	25.5	98	26.6	6	18.4	SE
	E	39.2				24.5			E	24.5				18.2	
T6032	W	39.9	120	26.7	6	24.3	SW	T9029d	W	38.3	110	30.4	6 ?	24.5	SW
	E	43.0				24.5			E	39.0				26.5	
T9025	W	35.8	128	32.7	6 ?	27.5	SW	T6018m	W	21.0	107	26.6	6	22.4	SE
	E	35.4				26.5			E	25.5				22.4	
T9029	W	38.0	81	22.7	6	22.5	FC	T9029m	W	40.9	116	30.2	6	28.6	SW
	E	40.8							E	38.3				30.2	

Table 4.2.1: Strength properties of test beams

a)

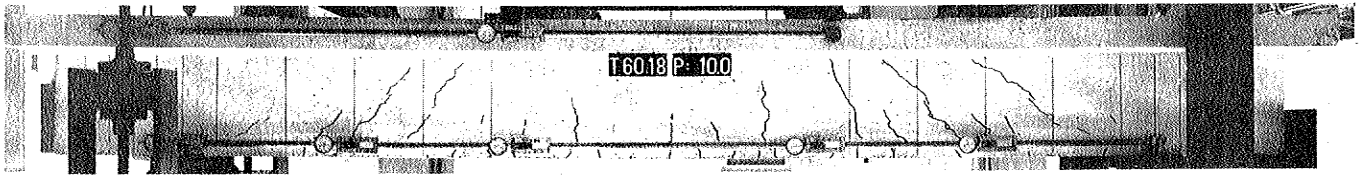

WEST EAST

b)

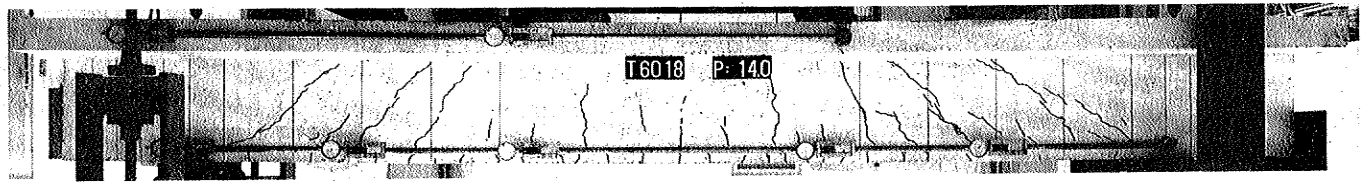

WEST EAST

c)

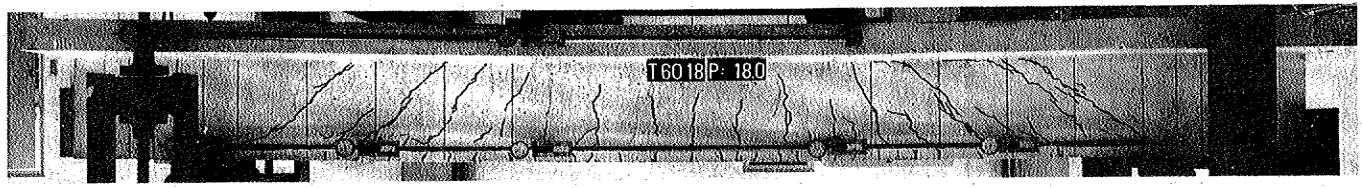

WEST EAST

d)

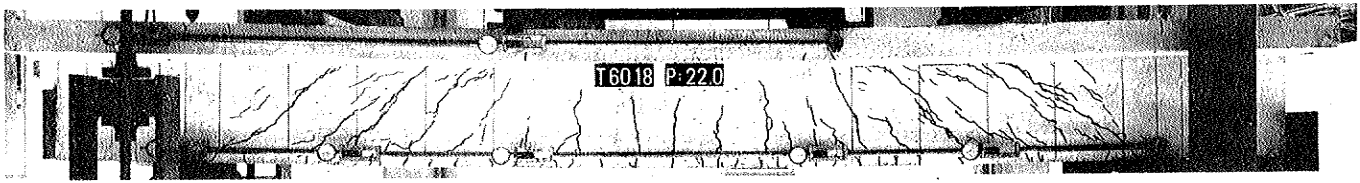

WEST EAST

e)

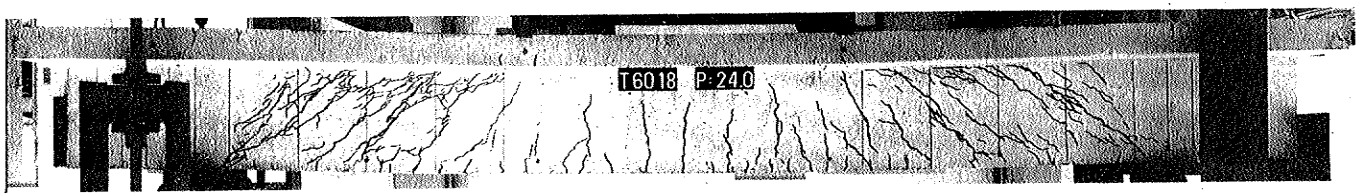

WEST EAST

Figure 4.2.1: Cracking patterns of Beam No.T6018

a) Load 10 Mp
b) Load 14 Mp
c) Load 18 Mp
d) Load 22 Mp
e) Load 24 Mp (after failure)

a)

b)

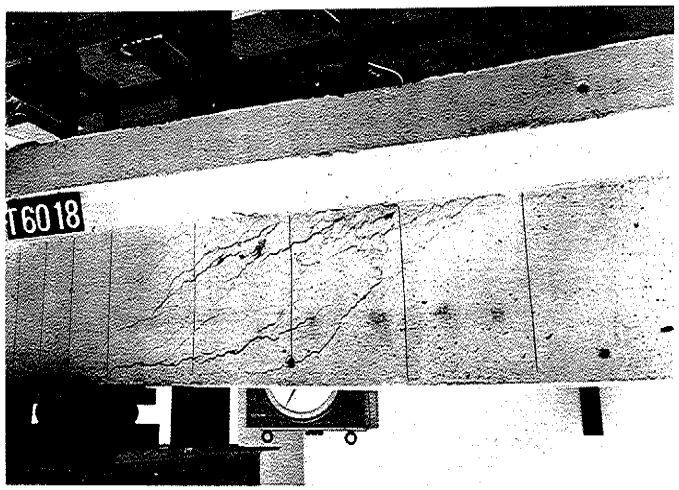

Figure 4.2.2: Close-up views of failures of Beam No.T6018.

a) First shear failure (WEST)
b) Second shear failure (EAST)

The shear cracking load V_{cr} is defined as the load step at which the first visible web crack appeared. Generally it was at the level of 6 Mp (i.e. at a load between 3 Mp and 6 Mp), somewhat increasing with increasing amount of stirrup reinforcement. A question mark in the table indicates that the beam was not thoroughly checked at the previous load stage, hence the first crack may have appeared earlier.

As the loading proceeded, it became obvious that the visible 'cracks' were carrying shear, through the formation of small crushing zones. The latter were barely visible, but could easily be felt with the fingertips on the surface of the web.

The development of the cracking is shown on Figures 4.2.1 for Beam No.T6018. The photographs have been turned upside down, so that the beam appears to be loaded from above.

At about 75% of the ultimate load, the shear 'cracks' extended into the flange. At this stage the deformations became considerable, and the beam assumed a characteristic S-shape with reversal of curvature at the supports. Just prior to failure, this lead to the formation of tensile cracks in the flange, as seen on Figure 4.2.1d and e.

Even quite close to the ultimate load, it remained an open question which shear span was going to fail first. Neither the location of the first visible crack, nor the extension of the cracks into the flange, could be taken as a guide. The only infallible sign was the appearance of the tensile flange cracks, mentioned above.

The ultimate load is defined as the maximum load recorded on the manometer, i.e. the load at which the pressostate is unable to keep up with the deformations. For some beams, failure was obtained during loading, but in most cases the load started to drop during a load stage. This does not appear from Table 4.2.1, owing to the fact that the load steps were not exactly 2 Mp (cf. the section below).

Of the 26 beams, 24 failed in shear. The two exceptions were Beam No.T5222, which was expected to get flexural failure (cf. Section 2.4), and Beam No.T9029, which untentionally got a very low concrete strength and failed in flexural compression. Right up to failure, however, both beams displayed the characteristic shear behaviour described above, including the tensile cracking of the flange.

On the other hand, Beam Nos. T5214 and T5218 showed yielding of the main reinforcement in the bending span, just before the shear failure. Also Beam No.T6029 behaved like it would fail in flexion, although no yielding of the main reinforcement was detected.

The shear failures were confined to the web, particularly to the level of the main reinforcement and to the junction of web and flange (cf. Figure 4.2.1e and the close-up views of Figure 4.2.2). The profusion of web crushing is probably due to the weakness of the concrete, which also accounts for the very ductile failure observed.

When the shear reinforcement in the two shear spans are different in strength, we would expect the weaker span to fail first. As seen from Table 4.2.1, this is not always the case. This reflects the fact that, especially with strong shear reinforcement, the ultimate load is more dependent upon concrete strength than upon the strength of shear reinforcement. While the latter is fairly well defined, the former is subject to unpredictable variations, as discussed in Section 3.1.

In the cases where two shear failures were obtained by the procedure described in Section 3.5, the second failure load was usually equal to or slightly higher than the first. This indicates that the second failure load may be used with confidence, although the moment distribution in the beam is somewhat different.

For Beam Nos. T6005 and T6010, a second shear test was not attempted. Beams Nos. T5214, T9032, and T9036 failed by shear in the same end as before. In the two latter cases, the failure took place in the former bending span, which was reinforced by five stirrups only rather than the usual seven (cf. Section 2.4). The ultimate shear forces on the three beams (24.9 Mp, 26.4 Mp, and 30.6 Mp, respectively) were equal to or higher than the first failure loads.

Beams Nos. T6018 and T9025 failed at a lower load by the second test. In both cases, the web was seriously strained during the first test (see Figure 4.2.1e). Furthermore, for Beam No. T6018 it cannot be excluded that the supposedly closed jack was applying an unknown load on the beam right up to failure (cf. Section 3.5).

It is worthy of note that the two failure loads for the same beam may differ by as much as 8%, although the strength properties of the two shear spans are supposedly identical. Thus a theoretical prediction of the load-carrying capacity must be subject to an unreliability of this order of magnitude.

4.3 Loads and deflexions

Figure 4.3.1 shows the loading history of Beam No. T6018. From 20 Mp the load steps were reduced to 1 Mp and at 21 Mp two scans were taken. As the deformations became negligible, the load was raised to 22 Mp and six readings taken. A single scan was taken at 23 Mp and the load was then increased to 24 Mp, but failure occurred before a scan could be performed at this load level.

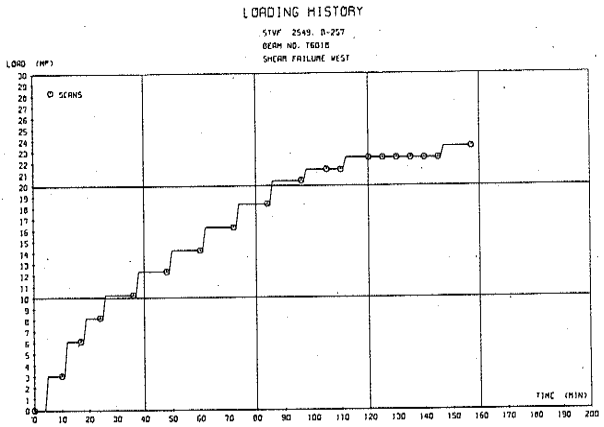

Figure 4.3.1: Loading history of Beam No.T6018

In subroutine LOADS, the load readings have been calibrated by means of data from a pressure cell. It turns out that the actual loads are 2% greater than the nominal. Thus, as seen on Figure 4.3.1, the load stage 20 Mp corresponds to an actual load of 20.4 Mp. In Table 4.2.1 of the preceding section, the actual failure loads are given. Whenever the load is given as an integer, say 20 Mp, we mean the nominal load or load stage.

Table 4.3.1: Deflexions of Beam No.T6018

DEFLEXIONS (CM) LOAD (MP)		EAST										WEST
0.0	*	0.0	0.0	0.0	0.0	0.0	0.0	0.0	0.0	0.0	0.0	0.0
3.1	*	0.0	0.02	0.05	0.07	0.08	0.10	0.10	0.07	0.05	0.03	0.0
6.1	*	0.0	0.08	0.16	0.22	0.26	0.28	0.28	0.22	0.15	0.09	0.0
8.2	*	0.0	0.12	0.24	0.34	0.40	0.42	0.42	0.33	0.23	0.13	0.0
10.3	*	0.0	0.17	0.33	0.47	0.55	0.57	0.57	0.46	0.32	0.18	0.0
12.4	*	0.0	0.22	0.42	0.61	0.72	0.76	0.74	0.60	0.42	0.22	0.0
14.3	*	0.0	0.27	0.52	0.76	0.89	0.93	0.91	0.74	0.52	0.27	0.0
16.3	*	0.0	0.32	0.64	0.95	1.11	1.15	1.12	0.92	0.63	0.32	0.0
18.4	*	0.0	0.38	0.78	1.16	1.36	1.42	1.39	1.14	0.77	0.38	0.0
20.4	*	0.0	0.46	0.95	1.42	1.68	1.75	1.71	1.40	0.96	0.45	0.0
21.4	*	0.0	0.50	1.03	1.55	1.84	1.91	1.87	1.55	1.03	0.49	0.0
21.4	*	0.0	0.51	1.05	1.58	1.86	1.95	1.90	1.58	1.04	0.49	0.0
22.5	*	0.0	0.56	1.16	1.74	2.06	2.15	2.11	1.75	1.15	0.53	0.0
22.5	*	0.0	0.56	1.16	1.76	2.10	2.19	2.14	1.78	1.17	0.54	0.0
22.5	*	0.0	0.57	1.19	1.80	2.13	2.22	2.18	1.81	1.19	0.54	0.0
22.5	*	0.0	0.57	1.20	1.81	2.15	2.24	2.20	1.83	1.20	0.54	0.0
22.5	*	0.0	0.57	1.22	1.83	2.16	2.27	2.22	1.85	1.21	0.55	0.0
22.5	*	0.0	0.58	1.22	1.84	2.18	2.28	2.23	1.86	1.22	0.56	0.0
23.5	*	0.0	0.63	1.32	1.99	2.30	2.49	2.35	2.04	1.33	0.59	0.0

The deflexions were measured at intervals of 300 mm along the beam, as described in Section 3.5. The results from Beam No.T6018 are listed in Table 4.3.1 and plotted on Figure 4.3.2. The deflexion curves lying close together correspond to the readings taken at constant load near failure.

Note the change of sign of the curvature near the supports. This effect is most marked in the western shear span, where the first failure took place. In one case (Beam No.T9071) the reversal of curvature was so drastic that it led to a decrease of deflexion near the support, as seen on Figure 4.3.3.

The behaviour of the beam close to the support is subject to further study in the section below.

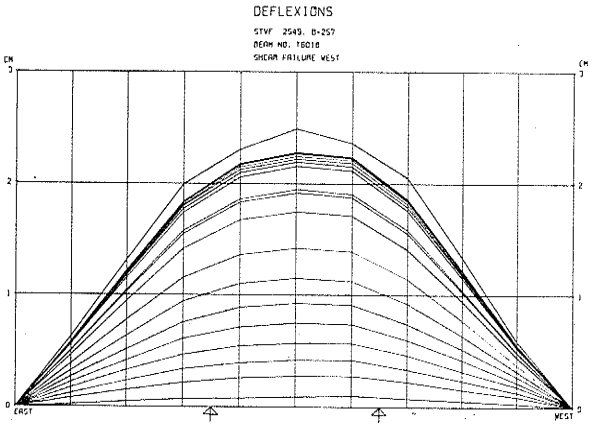

Figure 4.3.2: Deflexion curves for Beam No.T6018

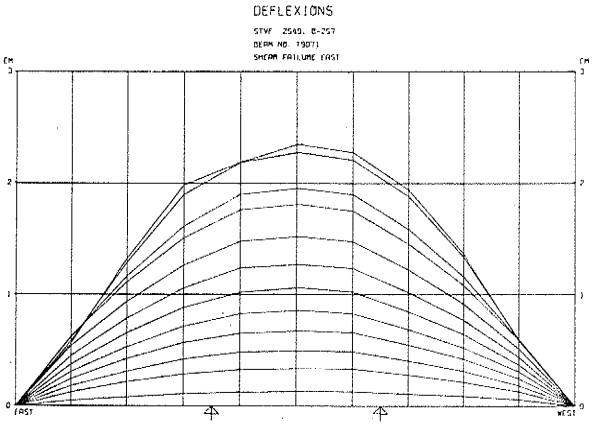

Figure 4.3.3: Deflexion curves for Beam No.T9071, showing reversal of deflexions close to support.

4.4 Dial gauge readings

Table 4.4.1 lists the readings of the 14 dial gauges for Beam No.T6018. The locations of the 7 dial gauges on each side of the beam is shown schematically on Figure 3.5.1. The readings on each side of the beam measured in $mm \cdot 10^{-2}$ are designated $u_1, u_2, \ldots, u_7$. The corresponding strains in % are found dividing by the gauge length in cm, thus:

$$\varepsilon_1 = \frac{u_1}{52.5} \quad , \quad \varepsilon_2 = \frac{u_2}{52.5} \quad , \quad \varepsilon_3 = \frac{u_3}{90} \quad , \quad \varepsilon_4 = \frac{u_4}{52.5}$$

$$\varepsilon_5 = \frac{u_5}{52.5} \quad , \quad \varepsilon_6 = \frac{u_6}{105} \quad , \quad \varepsilon_7 = \frac{u_7}{90}$$

The strains in the shear spans (i.e. ε_1, ε_2, ε_4, ε_5, and ε_6 for both sides) are plotted on Figure 4.4.1. Figure 4.4.2 shows the strains of the bending span (ε_3 and ε_7 for both sides).

Based upon the dial gauge data, subroutine DIALS calculates the curving of the bending span and the rotation of the beam end. The results are listed in Table 4.4.1 and plotted on Figure 4.4.3 for Beam No.T6018.

The curving α is defined as $\alpha = (u_3 + u_7)/z$. Here $z = 314$ mm is the vertical distance between the dial gauges in the bending span, and the average of the readings on the two sides of the beam is used. Thus α is the angle between the tangents to the beam at the loaded sections. The curvature in cm^{-1} is obtained dividing α by the bending span length 90cm.

The curvature is an almost linear function of the load on the beam. The only exceptions are the beams T52, where yielding of the main reinforcement was observed, as mentioned in Section 4.2. Figure 4.4.4 shows the curvatures of Beam No.T5214.

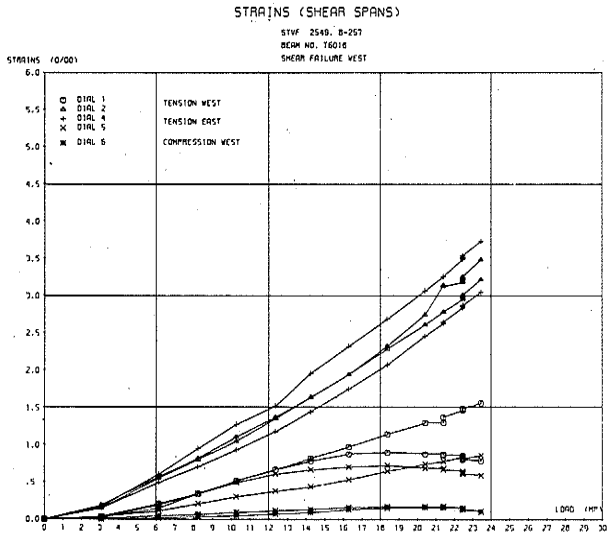

Figure 4.4.1: Strains in shear spans for Beam No.T6018

Table 4.4.1: Dial gauge readings, curvatures, and instaneous radii for Beam No.T6018

DIAL GAUGE READINGS (MM/100)

LOAD (MP)		NORTHERN SIDE 1	2	3	4	5	6	7	SOUTHERN SIDE 1	2	3	4	5	6	7	CURVATURES (0/00)	INSTANTANEOUS RADII (CM)
0.0	*	0	0	0	0	0	0	0	0	0	0	0	0	0	0	0.0	0.
3.1	*	2	10	21	9	2	0	5.	2	8	23	8	2	2	4	0.84	233.
6.1	*	11	30	54	32	6	2	10	10	29	58	26	8	5	8	2.07	162.
8.2	*	18	43	74	50	11	4	15	18	42	82	37	10	7	11	2.90	174.
10.3	*	27	58	97	67	16	5	20	27	55	105	49	26	10	15	3.77	175.
12.4	*	35	72	120	80	20	8	25	35	71	129	62	32	12	19	4.67	167.
14.3	*	41	86	141	103	23	10	32	43	86	151	76	35	14	24	5.56	218.
16.3	*	46	102	166	122	28	14	41	51	102	175	92	37	17	34	6.62	237.
18.4	*	47	122	190	141	34	16	53	60	120	195	109	38	18	57	7.88	298.
20.4	*	46	146	214	161	39	17	65	68	137	221	129	36	18	69	9.06	391.
21.4	*	46	165	227	171	41	17	72	68	146	236	138	36	18	77	9.75	324.
21.4	*	45	164	228	171	41	17	74	72	146	236	139	35	18	78	9.81	890.
22.5	*	45	167	241	183	44	16	81	77	155	251	149	34	16	84	10.46	861.
22.5	*	44	168	241	184	44	15	82	77	156	251	150	33	16	85	10.49	9999.
22.5	*	43	169	241	184	44	15	83	77	157	252	150	33	15	87	10.56	9999.
22.5	*	43	170	242	185	44	15	84	78	157	253	151	32	14	89	10.62	1457.
22.5	*	42	170	242	185	43	15	85	78	157	253	151	32	14	90	10.65	9999.
22.5	*	42	171	242	186	43	14	86	78	158	253	151	32	14	90	10.68	847.
23.5	*	41	183	254	196	45	11	91	82	169	266	160	31	11	94	11.23	490.

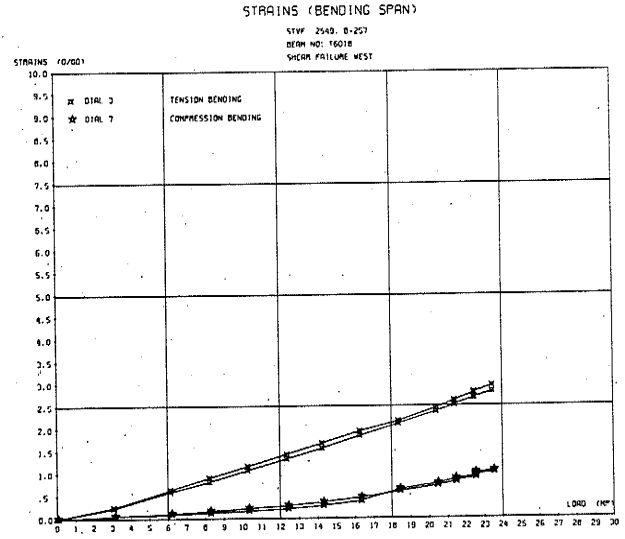

Figure.4.4.2: Strains in bending span for Beam No.T6018

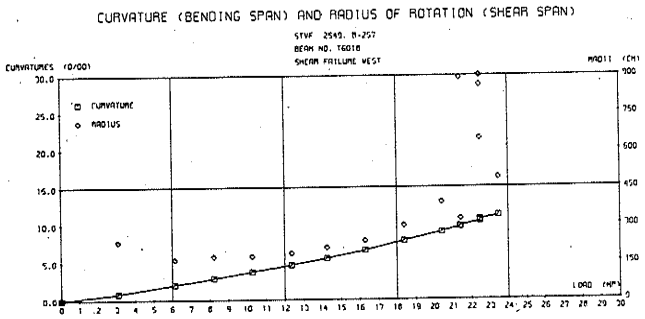

Figure 4.4.3: Curvatures and radii of rotation for Beam No.T6018

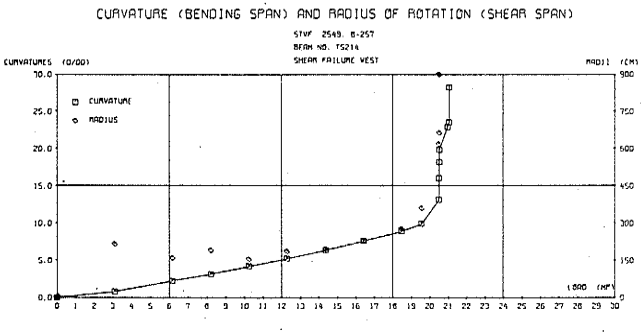

Figure 4.4.4: Curvatures and radii of rotation for Beam No.T5214

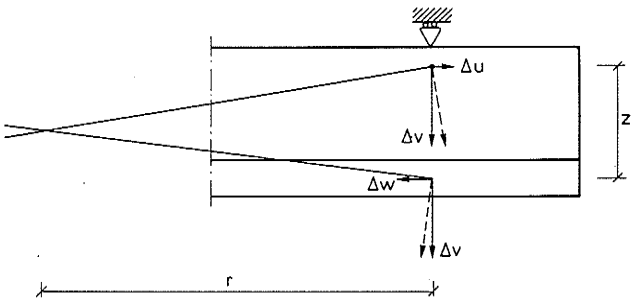

Figure 4.4.5: Calculation of instantaneous radius of rotation of the beam end

The instantaneous radius r of rotation of the beam end is found as sketched on Figure 4.4.5. Between two scans, the load deflects the distance Δv with respect to the support, the main reinforcement of the shear span increases the amount Δu in length, and the flange is compressed by Δw. We assume $r >> z$, $\Delta v >> \Delta u$, and $\Delta v >> \Delta w$. The radius of rotation of the support section with respect to the loaded section is then:

$$r = \frac{\Delta v}{\Delta u + \Delta w} \cdot z$$

Here $\Delta u = \Delta u_1 + \Delta u_2$ and $\Delta w = \Delta u_6$ (averages of the readings on the two beam faces). The deflexion of the load is not measured directly, but Δv is inserted as the average of the increases in deflexion of the points lying 150 mm on each side of the load. The instantaneous radii are listed in Table 4.4.1 and plotted on Figures 4.4.3 and 4. The value 9999 cm in the table means that r is infinite, $\Delta u + \Delta v$ being zero while Δv is non-zero. The range of the plot is limited to $r \leq 900$cm, hence values $r > 900$ cm are plotted as $r = 900$ cm.

We note that up to approximately 80% of the ultimate load, the radius remains fairly constant, if the order of magnitude 200 cm. Then it starts to increase and the very high values occur at the readings taken at constant load, when the deformations are due to plastic flow and/or redistribution of stresses.

This picture is the same for all the beams, including the ones (Beams Nos.T5222 and T9029) which failed in flexion.

4.5 Stirrup strains and forces

Table 4.5.1: Electrical resistance gauge strains for Beam No.T6018

ELECTRICAL GAUGE STRAINS (0/00)

LOAD (MP)		STIRRUP 1		STIRRUP 2		STIRRUP 3		STIRRUP 4	
0.0	*	0.0	0.0	0.0	0.0	0.0	0.0	0.0	0.0
3.1	*	0.00	0.0	0.01	0.00	-0.00	-0.01	0.00	0.01
6.1	*	0.14	0.09	0.09	0.07	0.12	0.17	0.04	0.06
8.2	*	0.24	0.24	0.16	0.15	0.23	0.30	0.10	0.15
10.3	*	0.48	0.36	0.27	0.21	0.46	0.53	0.16	0.21
12.4	*	0.59	0.46	0.31	0.32	0.56	0.66	0.26	0.32
14.3	*	0.67	0.52	0.42	0.47	0.66	0.74	0.38	0.45
16.3	*	0.76	0.68	0.59	0.67	0.98	0.84	0.52	0.61
18.4	*	0.94	0.77	0.77	0.89	0.94	0.96	0.68	0.79
20.4	*	1.14	0.96	0.98	1.11	1.14	1.05	0.78	1.01
21.4	*	1.22	1.06	0.94	1.11	1.24	1.08	1.12	1.09
21.4	*	1.22	1.07	0.94	1.22	1.25	1.09	1.14	1.10
22.4	*	1.31	1.21	1.02	1.34	1.37	1.12	1.29	1.18
22.5	*	1.31	1.23	1.03	1.35	1.38	1.12	1.31	1.19
22.5	*	1.33	1.24	1.04	1.35	1.39	1.11	1.32	1.20
22.5	*	1.33	1.25	1.05	1.35	1.40	1.11	1.32	1.21
22.5	*	1.33	1.26	1.05	1.36	1.41	1.10	1.32	1.22
22.5	*	1.33	1.27	1.06	1.36	1.41	1.10	1.32	1.23
23.5	*	1.48	1.42	1.15	1.47	1.56	1.13	1.39	1.33

Table 4.5.2: Stirrup strains for Beam No.T6018

AVERAGE STIRRUP STRAINS (0/00)

LOAD (MP)		STIRRUP 1	STIRRUP 2	STIRRUP 3	STIRRUP 4
0.0	*	0.0	0.0	0.0	0.0
3.1	*	0.00	0.01	-0.01	0.00
6.1	*	0.12	0.08	0.14	0.05
8.2	*	0.29	0.15	0.26	0.12
10.3	*	0.42	0.22	0.49	0.18
12.4	*	0.52	0.32	0.61	0.29
14.3	*	0.59	0.45	0.70	0.42
16.3	*	0.70	0.63	0.91	0.56
18.4	*	0.86	0.83	0.95	0.74
20.4	*	1.05	1.02	1.09	0.99
21.4	*	1.14	1.08	1.17	1.10
21.4	*	1.14	1.08	1.17	1.12
22.5	*	1.26	1.18	1.24	1.23
22.5	*	1.27	1.19	1.25	1.25
22.5	*	1.29	1.20	1.25	1.26
22.5	*	1.29	1.20	1.25	1.27
22.5	*	1.30	1.21	1.26	1.27
22.5	*	1.30	1.21	1.26	1.28
23.5	*	1.43 YIELD	1.31	1.31	1.36

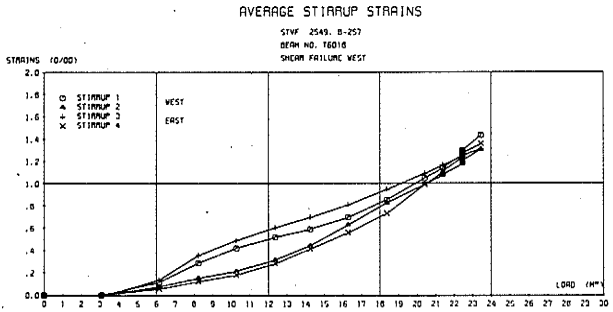

Figure 4.5.1: Stirrup strain curves for Beam No.T6018

As described in Section 3.3, the force- strain curves of the stirrups are idealized to perfectly plastic behaviour. Thus the yield strain ε_Y is defined as $\varepsilon_Y = P_Y/E_S$, P_Y and E_S being the yield force and the force-strain modulus, respectively. Comparing Tables 3.1.1 and 3.3.1, the yield strain of each individual gauge stirrup is found. The yield strain is approximately 1.5% for the mild steel and 2.8% for the cold-drawn steel.

The readings of the eight electrical resistance strain gauges on Beam No.T6018 are listed in Table 4.5.1. The gauge strains for the two gauges on each stirrup are combined to yield the average stirrup strains, displayed in Table 4.5.2 and plotted on Figure 4.5.1. The stirrup strains remain negligible until the shear cracking occurs. Then the strains increase almost proportionally to the load, at least as long as scans are taken. No yielding of the stirrups is observed on Figure 4.5.1, but one western stirrup did just reach the yield strain, cf. Table 4.5.2.

Figure 4.5.1 shows that the stirrup strains do increase a little during the scans taken at constant load. This indicates that a redistribution of stresses is taking place when the beam as such is yielding, i.e. deforming under constant load.

We would expect the stirrups of the beams with little shear reinforcement to yield at failure. The fact that in many cases no yield was registered by the strain gauges was considered so puzzling that an extra calibration of the gauges and the equipment was made (cf. Section 3.3). This doublecheck confirmed the results in every respect. We shall return to the question of stirrup yield in the following section.

The bending of the stirrups is measured by the difference between the strains of the two gauges on each stirrup. The differences (actually half the differences) are listed in Table 4.5.3 and plotted on Figure 4.5.2 for Beam No.T6018.

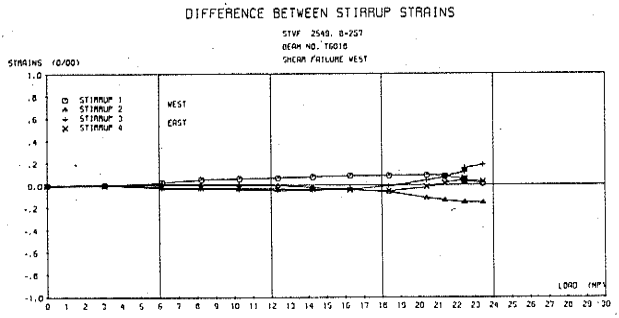

Figure 4.5.2: Stirrup bending curves for Beam No.T6018

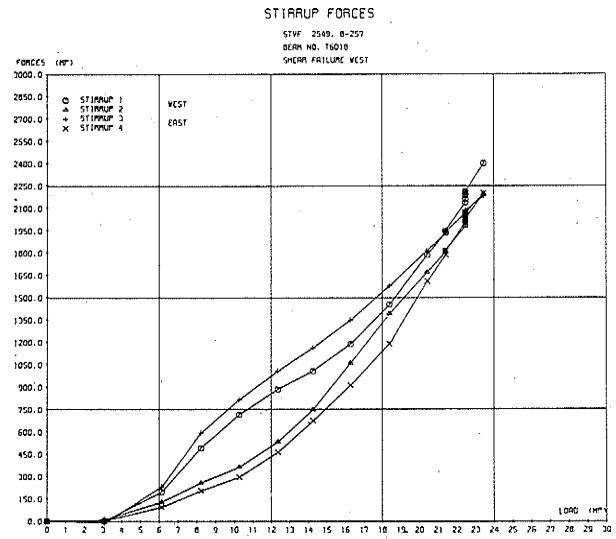

Figure 4.5.3: Stirrup force curves for Beam No.T6018

Table 4.5.3: Stirrup bending for Beam No.T6018

DIFFERENCE BETWEEN STIRRUP STRAINS (0/00)

LOAD (MP)	STIRRUP 1	STIRRUP 2	STIRRUP 3	STIRRUP 4
0.0	0.0	0.0	0.0	0.0
3.1	0.00	0.00	0.00	-0.00
6.1	0.03	0.01	-0.02	-0.02
8.2	0.05	0.01	-0.03	-0.02
10.3	0.06	0.00	-0.04	-0.03
12.4	0.07	0.00	-0.05	-0.03
14.3	0.07	-0.02	-0.04	-0.03
16.3	0.08	-0.04	-0.03	-0.04
18.4	0.08	-0.06	-0.01	-0.05
20.4	0.09	-0.12	0.05	-0.01
21.4	0.08	-0.14	0.07	0.01
21.4	0.07	-0.14	0.08	0.02
22.5	0.05	-0.16	0.12	0.05
22.5	0.04	-0.16	0.13	0.06
22.5	0.05	-0.16	0.14	0.00
22.5	0.04	-0.16	0.15	0.06
22.5	0.03	-0.15	0.15	0.05
22.5	0.03	-0.15	0.16	0.05
23.5	0.01	-0.16	0.18	0.03

Table 4.5.4: Stirrup forces for Beam No.T6018

STIRRUP FORCES (KP)

LOAD (MP)	STIRRUP 1	STIRRUP 2	STIRRUP 3	STIRRUP 4
0.0	0.0	0.0	0.0	0.0
3.1	5.0	1.7	-10.1	5.7
6.1	199.5	130.6	234.9	97.6
8.2	492.9	259.7	527.3	288.8
10.3	719.1	385.1	819.1	238.5
12.4	886.4	535.5	1010.5	465.5
14.3	1088.1	749.6	1169.9	670.3
16.3	1180.1	1032.3	1351.2	814.0
18.4	1453.5	1392.4	1580.3	1191.3
20.4	1786.1	1869.7	1815.5	1611.5
21.4	1936.1	1807.6	1935.5	1787.8
21.4	1946.5	1817.9	1942.7	1812.4
22.5	2138.9	1977.8	2065.9	2009.9
22.5	2120.3	1986.9	2073.2	2026.1
22.5	2167.0	2010.1	2077.5	2040.2
22.5	2194.4	2020.4	2081.9	2052.9
22.5	2201.8	2029.2	2084.8	2062.8
22.5	2210.7	2032.1	2086.2	2069.9
23.5	2400.0	2196.5	2161.9	2201.5

The stirrup forces are found by multiplying the stirrup strains by the force-strain modulus for each stirrup. When the stirrup strain exceed the yield strain, the stirrup force is put equal to the yield force, but as explained above, this only happens in a few cases. For Beam No.T6018, the stirrup forces are listed in Table 4.5.4 and plotted on Figure 4.5.3.

4.6 Yielding of stirrups

As mentioned in Section 3.5, only the stirrups were scanned during the second test of the beams. The readings were analysed by the programme RELOAD (cf. Section 4.1), and the results were examined to determine if the stirrups of the shear span which failed first had received any permanent strains, and if yielding of the stirrups of the remaining span was recorded.

Table 4.6.1: Analysis of stirrup strains at second test of Beam No.T6018

T6018 RELOADING OF EASTERN SHEAR SPAN

SCANS										
12.48	500*20	1*20	-1526*51	-1527*51	-1522*51	-1523*51	-1522*51	-1525*51	-1479*51	-1520*51	2*20
15.32	500*20	309*20	-722*51	-486*51	-897*51	-757*51	-800*51	-1060*51	-801*51	-833*51	309*20
15.37	501*20	371*20	-750*51	-525*51	-923*51	-782*51	-780*51	-1044*51	-791*51	-824*51	371*20
15.42	500*20	433*20	-773*51	-553*51	-943*51	-803*51	-755*51	-1021*51	-777*51	-811*51	433*20
15.47	501*20	465*20	620*51	600*51	600*51	600*51	600*51	-767*51	-1031*51	-787*51	-817*51	465*20
15.52	501*20	556*20	620*51	600*51	600*51	600*51	600*51	-709*51	-976*51	-746*51	-782*51	556*20
15.57	501*20	618*20	600*51	600*51	600*51	600*51	600*51	-661*51	-940*51	-700*51	-745*51	618*20
16.02	501*20	680*20	600*51	600*51	600*51	600*51	600*51	-614*51	-916*51	-695*51	-654*51	680*20

GAUGE STRAINS (1/00)

TIME	LOAD (MP)	GAUGE 1	GAUGE 2	GAUGE 3	GAUGE 4	GAUGE 5	GAUGE 6	GAUGE 7	GAUGE 8
12.48	0.0	0.00	0.00	0.00	0.00	0.00	0.00	0.00	0.00
15.32	10.2	1.40	1.82	1.69	1.34	1.26	0.81	1.18	1.20
15.37	12.2	1.36	1.75	1.65	1.29	1.30	0.84	1.25	1.22
15.42	14.3	1.38	1.77	1.61	1.26	1.34	0.88	1.23	1.24
15.47	16.4	3.71	3.71	3.70	3.70	1.32	0.86	1.21	1.23
15.52	18.4	3.71	3.71	3.70	3.70	1.42	0.58	1.28	1.29
15.57	20.4	3.71	3.71	3.70	3.70	1.50	1.02	1.36	1.35
16.02	22.5	3.71	3.71	3.70	3.70	1.58	1.06	1.37	1.51

STIRRUP STRAINS (0/00.)

12.48	0.0	0.00	0.00	0.00	0.00	0.00	0.00
15.32	10.2	1.61	1.21	1.21	1.04	1.07	1.19
15.37	12.2	1.20	1.17	1.17	1.11	1.11	1.21
15.42	14.3	1.61	1.13	1.13	1.09	1.09	1.23
15.47	16.4	3.71	3.70	3.70	3.70	1.19	1.28
15.52	18.4	3.71	3.70	3.70	3.70	1.26	1.35
15.57	20.4	3.71	3.70	3.70	3.70	1.38	1.44
16.02	22.5	3.71	3.71	3.70	3.70		

Table 4.6.1 shows the results of the second test for Beam No.T6018. The eastern span failed at 23 Mp, before scanning. The last scan, taken at 22 Mp, does not reveal any yielding, although stirrup 4 with a strain of 1.44‰ is very close.

We note, however, that at 10 Mp the western stirrups show strains of 1.61‰ and 1.21‰. At the following scans, the strains decrease, indicating that a steady state has not been reached after the first test. The gauges of the western stirrups were disconnected after scanning at 14 Mp. At any rate, we can conclude that stirrup 1 has been yielding. As for stirrup 2, yielding is probable, but not certain.

Beam Number	Failure Mode	WEST 1	WEST 2	EAST 3	EAST 4	Yield	Beam Number	Failure Mode	WEST 1	WEST 2	EAST 3	EAST 4	Yield
T5214	SW	0	0	0	0	(0)	T9032	SE	0	0	0	0	(0)
		-	-	(0)	(0)				0	0	0	B	
T5218	SE	0	0	0	0	Y	T9036	SW	0	0	0	0	0
		0	0	Y	Y				0	0	0	0	
T5222	FT	0	0	0	0	0	T9040	SE	0	0	0	0	0
									0	0	0	0	
T6005	SEW	0	0	0	Y	Y	T9043	SE	0	0	0	0	(0)
									0	0	0	B	
T6010	SE	Y	0	0	0	Y	T9047	SW	(0)	0	0	0	(0)
									(0)	0	0	0	
T6014	SE	Y	0	(0)	-	Y	T9060	SW	0	0	0	0	0
		-	Y	Y	-				-	0	0	0	
T6018	SW	(0)	0	0	0	Y	T9065	SE	0	0	0	0	0
		Y	(0)	0	(0)				0	0	-	-	
T6022	SE	0	Y	Y	0	Y	T9071	SE	0	0	0	0	0
		0	Y	-	0				0	0	0	0	
T6025	SW	0	0	0	0	0	T9078	SE	0	0	0	0	0
		-	-	0	0				0	0	0	0	
T6029	SE	0	0	0	0	Y	T6018d	SE	0	0	0	0	0
		0	Y	(0)	0				-	0	0	-	
T6032	SW	0	0	0	0	(0)	T9029d	SW	0	0	0	0	Y
		B	0	0	0				Y	Y	0	0	
T9025	SW	(0)	(0)	0	(0)	Y	T6018m	SE	0	0	0	0	Y
		Y	Y	0	Y				0	(0)	Y	(0)	
T9029	FC	0	0	0	0	0	T9029m	SW	Y	Y	0	0	Y
									-	-	0	0	

Table 4.6.2: Recordings of stirrup yield at first and second testing of beams.

0 : No yielding detected
(0) : Possible yielding detected
Y : Yielding recorded

- : Strain gauges disconnected or inoperable
B : Permanent strain of stirrup in connection with pronounced bending

The outcome of the investigation of stirrup yield for all the test beams is shown in Table 4.6.2. Corresponding to each beam, the table lists the failure mode (cf. Section 4.2) and the results of the examination of each stirrup during first (top line) and second (bottom line) test. The symbols used are explained in the caption to the table. Finally the beam is classified according to yielding of stirrups (certain, possible, or not recorded). We note that the beams with identification numbers greater than 29 showed no certain yielding, whereas the rest of the beams did. Exceptions are the flexural failures and Beams No.T5214 and T6025, where the gauges on the western stirrups were disconnected before reloading of the eastern shear span.

4.7 Ultimate loads

Table 4.7.1: Test results from the five series T

SERIE T52 ABK 1973/74

SHEAR DEPTH CALCULATED FROM CENTROID OF MAIN REINFORCEMENT TO CENTRE OF FLANGE

BEAM NO.		WEB WIDTH B CM	SHEAR DEPTH H CM	STIRRUP STRENGTH SY KP/SQCM	CONCRETE STRENGTH SIGMAC KP/SQCM	FAILURE LOAD V MP	PSI SY/SIGMAC 0/0	TAU/SIGMAC V/B/H/SIGMAC 0/0	NU 0/0
T5214	W	20.0	31.4	19.4	109.0	21.9	17.8	32.0	75.3
T5218	W	20.0	31.4	24.4	105.0	22.4	23.2	34.0	72.9
T5218	E	20.0	31.4	25.4	105.0	21.7	24.2	32.9	69.0
T5222		20.0	31.4	28.9	105.0	21.2	27.5	32.2	FLEXURAL FAILURE

WEB EFFECTIVENESS GIVING CLOSEST FIT: NU = 71.8 0/0
NUMBER OF ITERATIONS: 11
COEFFICIENT OF VARIATION: 2.7 0/0

SERIE T60 ABK 1973/74

SHEAR DEPTH CALCULATED FROM CENTROID OF MAIN REINFORCEMENT TO CENTRE OF FLANGE

BEAM NO.		WEB WIDTH B CM	SHEAR DEPTH H CM	STIRRUP STRENGTH SY KP/SQCM	CONCRETE STRENGTH SIGMAC KP/SQCM	FAILURE LOAD V MP	PSI SY/SIGMAC 0/0	TAU/SIGMAC V/B/H/SIGMAC 0/0	NU 0/0
T6005	W	20.0	31.4	6.9	108.0	16.1	6.4	23.7	94.6
T6005	E	20.0	31.4	7.1	108.0	16.1	6.6	23.7	92.3
T6010	E	20.0	31.4	14.2	105.0	19.4	13.5	28.4	77.5
T6014	W	20.0	31.4	19.5	113.0	22.2	17.2	33.1	82.5
T6014	E	20.0	31.4	19.9	116.0	22.7	17.2	31.2	73.8
T6018	W	20.0	31.4	24.6	112.0	24.5	21.9	34.6	77.8
T6018	E	20.0	31.4	25.7	113.0	23.5	22.9	33.4	71.5
T6022	W	20.0	31.4	30.7	106.0	23.9	29.0	35.9	73.5
T6022	E	20.0	31.4	29.7	106.0	22.4	28.0	33.6	68.4
T6025	W	20.0	31.4	34.7	104.0	22.4	33.4	34.9	69.6
T6025	E	20.0	31.4	35.6	104.0	24.2	34.2	37.1	74.5
T6029	W	20.0	31.4	39.8	108.0	26.5	36.9	39.1	76.3
T6029	E	20.0	31.4	39.2	108.0	24.5	36.3	36.1	72.2
T6032	W	20.0	31.4	39.9	120.0	24.3	33.2	32.2	64.5
T6032	E	20.0	31.4	43.0	120.0	24.5	35.8	32.5	65.0

WEB EFFECTIVENESS GIVING CLOSEST FIT: NU = 71.8 0/0
NUMBER OF ITERATIONS: 47
COEFFICIENT OF VARIATION: 5.7 0/0

SERIE T90 ABK 1973/74

SHEAR DEPTH CALCULATED FROM CENTROID OF MAIN REINFORCEMENT TO CENTRE OF FLANGE

BEAM NO.		WEB WIDTH B CM	SHEAR DEPTH H CM	STIRRUP STRENGTH SY KP/SQCM	CONCRETE STRENGTH SIGMAC KP/SQCM	FAILURE LOAD V MP	PSI SY/SIGMAC 0/0	TAU/SIGMAC V/B/H/SIGMAC 0/0	NU 0/0
T9025	W	20.0	31.4	35.8	128.0	27.5	28.0	34.2	69.8
T9025	E	20.0	31.4	35.4	128.0	29.5	27.7	33.0	67.0
T9029		20.0	31.4	38.0	81.0	23.5	46.9	44.0	FLEXURAL FAILURE
T9032	E	20.0	31.4	47.6	101.0	26.3	47.1	41.5	68.9
T9036	W	20.0	31.4	51.6	104.0	28.5	48.4	43.6	68.4
T9040	W	20.0	31.4	49.5	115.0	26.5	43.0	36.7	73.4
T9040	E	20.0	31.4	52.9	115.0	25.4	45.2	35.2	70.3
T9043	W	20.0	31.4	55.2	108.0	28.5	52.6	43.4	86.7
T9043	E	20.0	31.4	56.7	108.0	27.6	54.0	41.4	83.7
T9047	W	20.0	31.4	62.3	129.0	28.5	48.3	35.3	70.6
T9047	E	20.0	31.4	59.9	129.0	30.4	46.4	37.2	74.5
T9060	W	20.0	31.4	68.9	121.0	24.5	56.9	32.3	64.5
T9060	E	20.0	31.4	68.9	121.0	24.3	56.9	32.0	64.0
T9065	W	20.0	31.4	70.9	109.0	24.5	65.1	32.2	76.5
T9065	E	20.0	31.4	78.9	102.0	24.5	77.4	32.2	76.5
T9071	W	20.0	31.4	88.4	111.0	26.5	79.6	35.0	76.6
T9071	E	20.0	31.4	80.4	111.0	24.5	72.3	32.2	70.9
T9078	W	20.0	31.4	98.5	115.0	26.6	85.7	33.6	79.2
T9078	E	20.0	31.4	98.5	115.0	26.5	85.7	36.7	73.4

WEB EFFECTIVENESS GIVING CLOSEST FIT: NU = 75.0 0/0
NUMBER OF ITERATIONS: 6
COEFFICIENT OF VARIATION: 8.9 0/0

SERIE TD ABK 1974

SHEAR DEPTH CALCULATED FROM CENTROID OF MAIN REINFORCEMENT TO CENTRE OF FLANGE

BEAM NO.		WEB WIDTH B CM	SHEAR DEPTH H CM	STIRRUP STRENGTH SY KP/SQCM	CONCRETE STRENGTH SIGMAC KP/SQCM	FAILURE LOAD V MP	PSI SY/SIGMAC 0/0	TAU/SIGMAC V/B/H/SIGMAC 0/0	NU 0/0
T6018D	W	20.0	31.4	25.5	98.0	18.4	26.0	29.9	60.4
T6018D	E	20.0	31.4	24.5	98.0	18.2	25.0	29.6	60.0
T9029D	W	20.0	31.4	38.3	110.0	24.5	34.8	35.5	70.9
T9029D	E	20.0	31.4	39.0	110.0	26.5	35.5	38.4	77.0

WEB EFFECTIVENESS GIVING CLOSEST FIT: NU = 69.0 0/0
NUMBER OF ITERATIONS: 23
COEFFICIENT OF VARIATION:10.5 0/0

SERIE TM ABK 1974

SHEAR DEPTH CALCULATED FROM CENTROID OF MAIN REINFORCEMENT TO CENTRE OF FLANGE

BEAM NO.		WEB WIDTH B CM	SHEAR DEPTH H CM	STIRRUP STRENGTH SY KP/SQCM	CONCRETE STRENGTH SIGMAC KP/SQCM	FAILURE LOAD V MP	PSI SY/SIGMAC 0/0	TAU/SIGMAC V/B/H/SIGMAC 0/0	NU 0/0
T6018M	W	20.0	31.4	21.0	107.0	22.4	19.6	33.3	76.2
T6018M	E	20.0	31.4	25.5	107.0	22.4	23.8	33.3	70.5
T9029M	W	20.0	31.4	40.9	116.0	28.6	35.3	39.3	79.6
T9029M	E	20.0	31.4	38.3	116.0	30.2	33.0	41.5	85.1

WEB EFFECTIVENESS GIVING CLOSEST FIT: NU = 79.2 0/0
NUMBER OF ITERATIONS: 19
COEFFICIENT OF VARIATION: 5.4 0/0

As described in Section 4.2, the 26 beam tests yielded 44 shear failure loads plus 2 flexural failure loads, grouped in five series: T52 (3+1 failures), T60 (15 failures), T90 (18+1 failures), Td (4 failures), and Tm (4 failures). The test results are summarized in Table 4.7.1. The table lists the strength parameters, the ultimate loads, and the non-dimensional parameters ψ and τ/σ_c, introduced in Section 1.1. According to the web crushing criterion, the points $(\psi, \tau/\sigma_c)$ should lie on a MOHR's circle with diameter ν or on its horizontal tangent. The value ν given in Table 4.7.1 for each test is the diameter of the MOHR's circle on which the particular point $(\psi, \tau/\sigma_c)$ is located. For points with $\psi > \tau/\sigma_c$, we have put $\nu = 2\tau/\sigma_c$ assuming that the point is lying on the tangent. The average is used as the start value for ν in the programme EXP, described in Section 4.1, which calculates the best web effectiveness ν for each of the five series. The results are given in Table 4.7.1.

The test results for the five series are plotted on Figure 4.7.1. The curves represent the web crushing criteria giving closest fit, as explained above. The two flexural failures are included in the table and on the figures. The value ψ used is the one corresponding to the weakest shear span. The flexural failures are omitted from the calculation of the web effectiveness.

a)

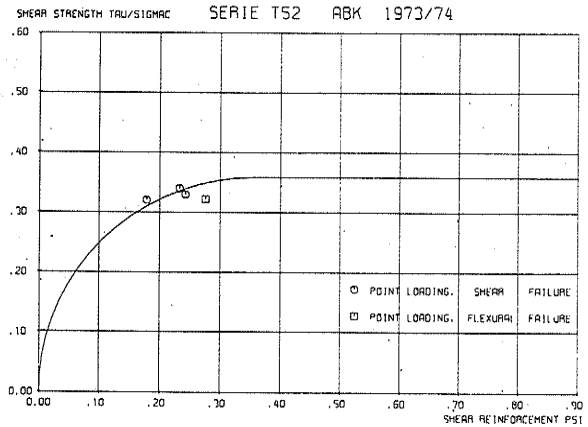
SHEAR STRENGTH TAU/SIGMAC
SERIE T52 ABK 1973/74
.60
.50
.40
.30
.20
.10
0.00
0.00 .10 .20 .30 .40 .50 .60 .70 .80 .90
SHEAR REINFORCEMENT PSI
POINT LOADING. SHEAR FAILURE
POINT LOADING. FLEXURAL FAILURE

b)

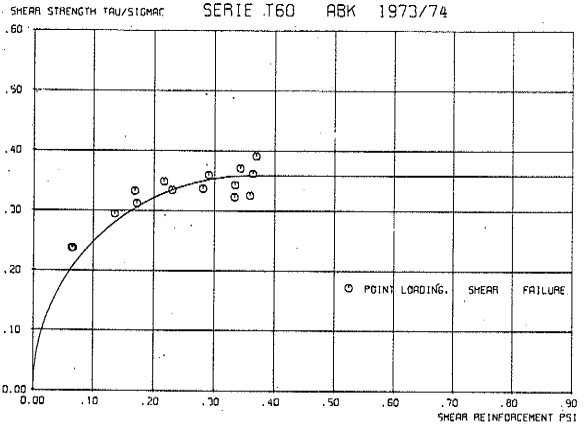
SHEAR STRENGTH TAU/SIGMAC
SERIE T60 ABK 1973/74
.60
.50
.40
.30
.20
.10
0.00
0.00 .10 .20 .30 .40 .50 .60 .70 .80 .90
SHEAR REINFORCEMENT PSI
POINT LOADING. SHEAR FAILURE

c)

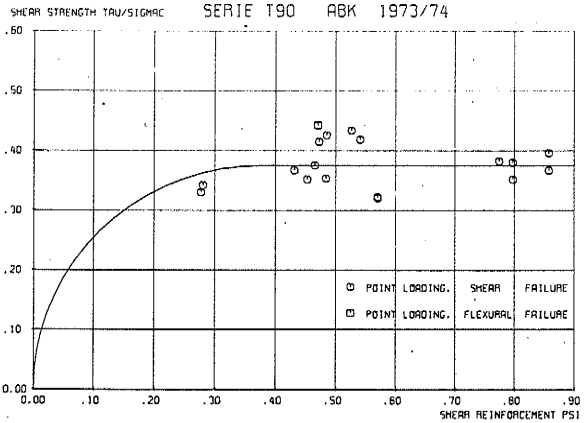
SHEAR STRENGTH TAU/SIGMAC
SERIE T90 ABK 1973/74
.60
.50
.40
.30
.20
.10
0.00
0.00 .10 .20 .30 .40 .50 .60 .70 .80 .90
SHEAR REINFORCEMENT PSI
POINT LOADING. SHEAR FAILURE
POINT LOADING. FLEXURAL FAILURE

d)

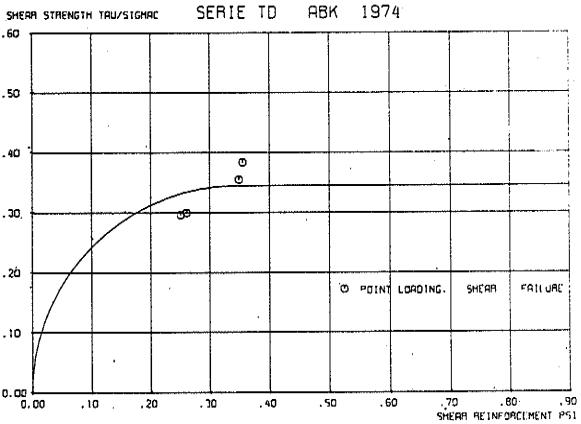

e)

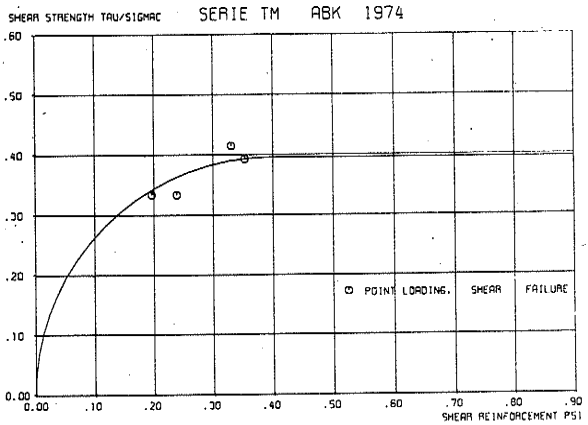

Figure 4.7.1: Test results for series T
(Shear depth: h*= z)

a) Series T52
b) Series T60
c) Series T90
d) Series Td
e) Series Tm

5. CONCLUSIONS

5.1 Failure mechanism

The behaviour of the beam, described in Section 4.2, follows the pattern staked out in Section 1.1. As seen on Figure 4.2.1a, the first shear cracks have an inclination of approximately 45° (cf. Figure 1.1.2a). Figures 4.2.1b, c, and d show the decreasing inclination of the subsequent cracks (cf. Figure 1.1.2b). On Figure 4.2.1d, note the appearance of tensile flange cracks, indicating that a yield zone has been formed (cf. Figure 1.1.2c). The decreasing inclination of the yield lines is seen on Figure 4.2.1e, which shows how the yield line starting at the western support on Figure 4.2.1d has been added a flatter branch (cf. Figure 1.1.2d).

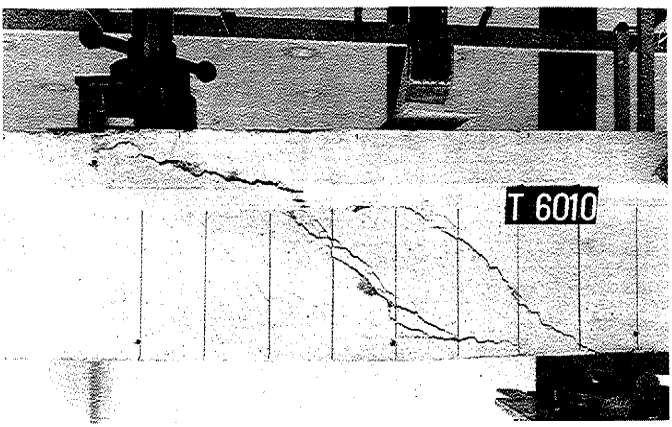

Figure 5.1.1: Failure of Beam No.T6010

The western span of Beam No.T6018 had a shear reinforcement degree of $\psi = 0.22$ (Table 4.7.1). With $\nu = 0.72$, the theoretical crack inclination φ (Section 1.1) is determined by:

$$\cot\varphi = \sqrt{\nu/\psi - 1} = 1.51$$

Hence the crack inclination should be $\varphi = 33.5^{\circ}$ and the yield line inclination $\theta = 2\varphi = 67^{\circ}$. While the former value does not seem far off, the yield lines observed on Figure 4.2.1c are obviously much flatter than 67° . This is bound up with another deviation from the predicted behaviour, viz. the fact that, as shown in Sections 4.5 and 4.6, the stirrups do not yield until immediately before failure, i.e. in stage IV. Thus we may conclude that the elastic strains of the stirrups are great enough to permit the formation of the yield lines in the concrete which are observed as early as in stage III (Figure 4.2.1d). Accordingly, the yield lines must be flatter than expected. Note, however, that if we define the angle θ as the inclination of the lines bounding the yield zone (Figure 1.1.1b), then the prediction $\theta = 67^{\circ}$ is not too bad. The extension of the yield zone is determined by the tensile flange cracks mentioned above, which indicate that a yield node in the flange has been formed.

The type of failure observed must be classified as web crushing. The distress of the web was most dominant for the strongly reinforced beams. The beams with little shear reinforcement tended to have the deformations concentrated in one or two yield lines. Figure 5.1.1 shows the failure of Beam No. T6010, which was the only case where a yield line proceeded through the compression flange. Traditionally, this failure would be described as 'diagonal tension failure'. It is evident from Figure 5.1.1, however, that substantial shear forces are transferred through the 'diagonal cracks'.

Figure 5.1.2: Second failure of Beam No.T9078

If the deformations are carried on long enough, the compression flange is eventually destroyed, as seen on Figure 5.1.2, showing the second shear failure of Beam No.T9078. To classify this failure as shear-compression would be misleading since the flange failure is obviously due to the excentric compression caused by the web deformations. We suspect many of the shear-compression failures reported in the literature to be of the same nature, but this claim will have to be supported by tests on beams with a stronger concrete.

The general behaviour of the beams (Section 4.2) and the deflexion curves (Section 4.3) substantiate proposition (1) of Section 2.1. A quantitative support is provided by the mea-

surements of the beam end rotations (Section 4.4). Since the value of the radius of rotation is found through division by a small quantity, it can only be taken to express the order of magnitude. Even so, the measurements clearly show that the rotation about the crack top, assumed by most shear failure theories, is almost nonexistent. Moreover, it appears that what little rotation there may be, is mainly due to elastic elongation of the main reinforcement and compression of the concrete flange. The measurements taken at constant load show the radius of rotation to be practically infinite, indicating that the failure mechanism is indeed a parallel translation of the loaded section with respect to the support section.

In the preceding analysis it has been taken for granted that the yield lines were traces of failure planes perpendicular to the plane of the beam. With the purpose of studying this question, two beams were cut through after failure at normal sections in the middle of the shear spans. The cross-section of Beam No.T6029 is shown on Figure 5.1.3, before and after the cracks have been traced by ink. Figure 5.1.4 shows the cross -section of Beam No.T6018d. In either case, the cut has been placed in the shear span which failed first, hence it cannot be excluded that some of the cracks observed were caused by the second shear test.

The photographs are most interesting, however, by the cracks that are missing. Thus we note that the cracking observed on the faces of the beam does not penetrate the web, but appears to be confined to a surface layer more or less identical with the concrete cover on the stirrups. Instead there seems to be one or more failure planes running obliquely through the web. There is no cracking at the centre bars, not even for Beam No. T6018d, where we would expect these bars to receive twice as much load from the stirrups as the corner bars (cf.Figure 2.2.2b). A possible explanation for the absence of cracks is that splitting is resisted by the transverse concrete compression balancing the tension in the horizontal stirrup legs.

a)

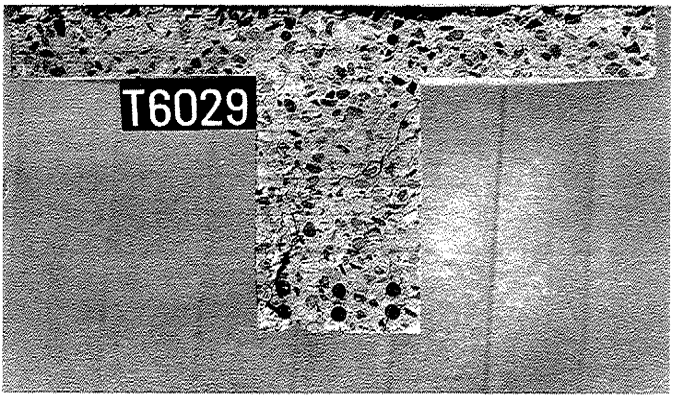

b)

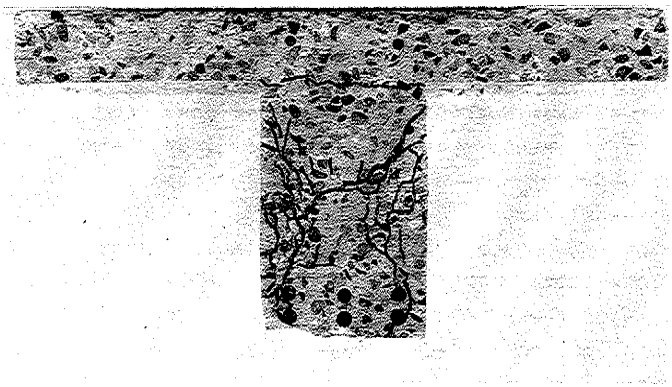

Figure 5.1.3: Normal section of Beam No.T6029 (Eastern shear span)

a) Before tracing of cracks

b) After tracing of cracks

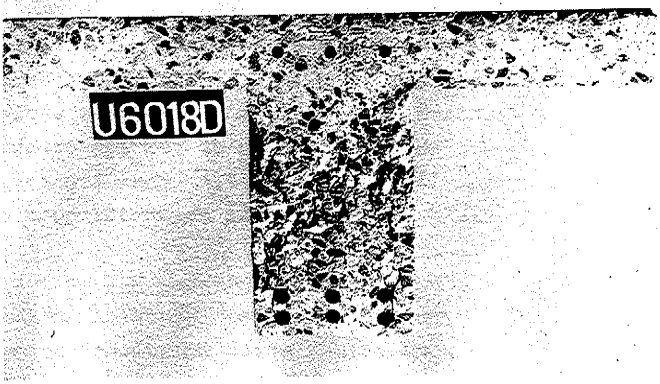

Figure 5.1.4: Normal section of Beam No.T6018d
(Eastern shear span)
(Mistakenly labelled U6018d)

Thus it may be concluded that in order to get a full understanding of the web failure mechanism, it is necessary to consider a three-dimensional yield pattern. We shall return to this question in Section 5.5.

5.2 Influence of main reinforcement strength

The series T52, T60, and T90 were made with different strengths of main reinforcement. Comparison of the ultimate loads (Table 4.7.1 and Figures 4.7.1a, b, and c) shows that the differences in web effectiveness ν are of the same order of magnitude as the standard deviations for the three series. Thus the tests support the implication of the web crushing criterion (proposition (2) of Section 2.1) that the strength of main reinforcement has no effect on the shear strength of the beam.

This conclusion may be substantiated somewhat more by statistical means. Our hypothesis is that the three series are samples from the same population, which we assume to be normal. The numbers N of observations, the sample means $\bar{x}$, and the sample variances s^2 are given in Table 5.2.1 based upon the values of Table 4.7.1. The variance is calculated from the coefficient of variation, and the mean is put equal to the best value of ν.

Series	N	$\bar{x}$	s	s^2
T52	3	71.8	1.94	3.76
T60	15	71.8	4.09	16.7
T90	18	75.0	6.68	44.6

Table 5.2.1: Sample means and variances for series T52, T60, and T90. (Shear depth: $h^* = z$)

Series	s_1^2/s_2^2	$F_{97.5}$	s_{12}	t_{12}	$t_{97.5}$
1: T60 2: T52	4.4	39.4	3.88	0	2.12
1: T90 2: T52	11.9	39.4	6.35	0.81	2.10
1: T90 2: T60	2.67	2.91	5.66	1.62	2.05

Table 5.2.2: F-test on sample variances and t-test on sample means

The differences of the variances are investigated by the F-test (cf. reference [8] pp. 193 ff.). Table 5.2.2 lists the variance ratios and the 97.5% fractile for the F-statistic (taken from reference [9]). In all three cases the F-value is greater than the variance ratio. Consequently, the sample variances are not different at the 95% significance level. An estimate of the common variance s_{12}^2 is then:

$$s_{12}^2 = \frac{(N_1-1)s_1^2 + (N_2-1)s_2^2}{N_1+N_2-2}$$

The values of the standard deviation s_{12} are given in Table 5.2.2.

The differences of the means are investigated by the t-test (reference [8] pp. 184 ff.). For each pair of samples, the quantity

$$t_{12} = \frac{|\bar{x}_1 - \bar{x}_2|}{s_{12}\sqrt{\frac{1}{N_1}+\frac{1}{N_2}}}$$

is calculated and compared with the 97.5% fractile of the t-statistic (Table 5.2.2). In all cases we have $t_{12} > t_{97.5}$, hence the means are not significantly different at the 95% level.

As a consequence of this result, the three test series are combined on a plot, Figure 5.2.1. The web effectiveness is $\nu = 73.9\%$, the coefficient of variation being 7.4%.

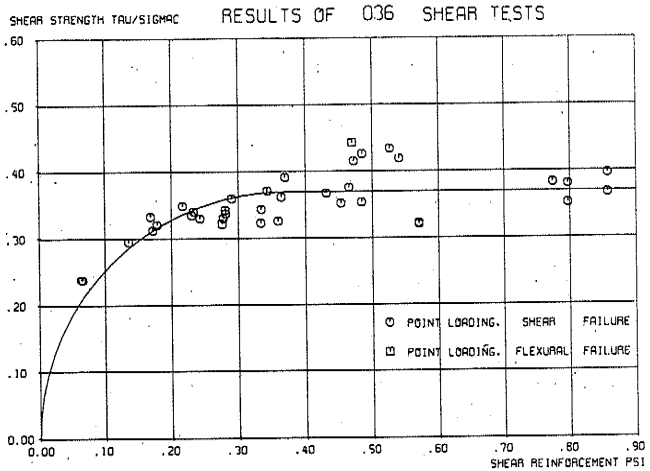

Figure 5.2.1: Test results for series T52, T60, and T90 (Shear depth = $h^* = z$)

Figure 5.2.2: Failure of Beam No.T5214

Of course, the proposition is only justified provided the main reinforcement is strong enough and well enough anchored to resist the tensile stringer force at all points of the shear span. When this is not the case, e.g. if the main reinforcement is curtailed, then we cannot expect the web crushing criterion to apply. Beams with curtailed reinforcement are the subject of a subsequent test series.

The design of main reinforcement according to the proposed theory is treated in reference [3]. When the main reinforcement is carried all the way through and well anchored, as is the case with the present test beams, then the shear strength should be given by the web crushing criterion with the full flexural capacity as an upper limit. This claim is supported by the results from series T52 (cf. Table 4.2.1 and Figure 4.7.1). The fact that the main reinforcement was yielding for these beams did apparently not reduce the ultimate load in shear. It may have had an effect on the failure mechanism, which seems to be a combination of flexure and shear, as seen on Figure 5.2.2, showing the failure of Beam No.T5214. Apparently the failure mechanism has involved some rotation in the yield lines (see also Figure 4.4.4).

5.3 Strong shear reinforcement

Beams Nos. T9060, T9065, T9071, and T9078 were made with stirrups of cold-drawn steel and had very high degrees of shear reinforcement. The behaviour of these beams was not different

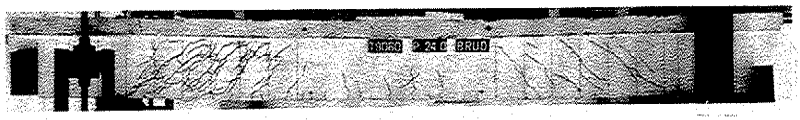

Figure 5.3.1: Failure of Beam No.T9060

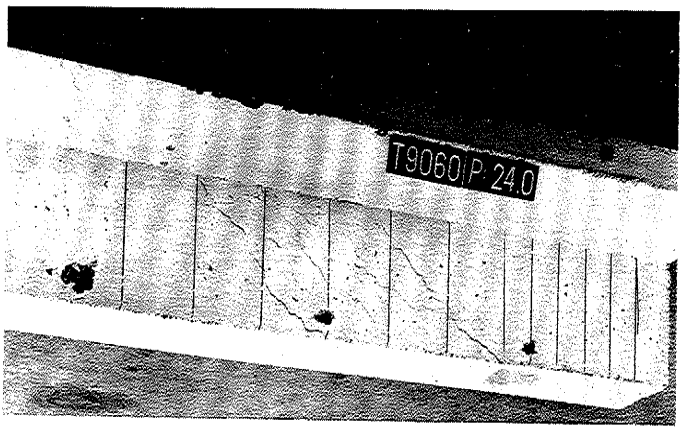

Figure 5.3.1: First failure of Beam No.T9060

a) Overall view
b) Detail

from that of the rest. Figure 5.3.1 shows the first failure of Beam No.9060. According to the web crushing criterion, the concrete cracks (i.e. the compression struts) should remain at an inclination of 45° to the beam axis, and the yield lines should be vertical, i.e. the limits of the yield zone (cf. Figure 1.1.1) should be planes normal to the beam axis. Judging from the close-up photograph of Figure 5.3.1b, the first claim seems to be true, whereas the second is not supported. As mentioned in Section 5.1, it appears that the elastic strains of the stirrups permit the formation of inclined yield lines in the concrete.

On Figure 4.7.1c it is seen that the ultimate loads of the four beams were almost equal in spite of the fact that the degree of shear reinforcement varied by approximately 50%. This supports the proposition (3) of Section 2.1 that the load-carrying capacity is independent upon the amount of shear reinforcement, provided the latter is sufficiently great.

The reason for this is that the concrete of the web fails before the stirrups are yielding. Thus the degree of shear reinforcement $\psi = \psi_1$ which is necessary for this situation to arise may be deduced from the observations of stirrup yield. Comparing Table 4.6.2 with Table 4.7.1, we note that the most strongly reinforced shear span for which yielding was recorded with certainty is the western span of Beam No.T6029, which had $\psi = 0.369$. The weakest shear span for which no yielding is observed is the western span of Beam No.T9040 with $\psi = 0.430$. Thus we deduce that the value of ψ_1 lies in the interval $0.37 < \psi_1 < 0.43$. The upper limit is unreliable, however, since failure to record stirrup yield constitutes no proof that yielding has not taken place.

The use of high strength stirrups is prohibited by most building codes for fear of excessive crack widths. Judging from the present tests, this concern seems unfounded, but on the other hand, the stirrups are far from yielding, and may therefore be expected to behave more or less like ordinary mild steel stirrups.

5.4 Effective shear depth

In Section 4.7, the ultimate loads were analysed using as shear depth the internal moment lever arm z. As discussed in Section 1.2 it might be more appropriate to use the quantities h_s or h_w. In Table 5.4.1, the web effectiveness ν and the coefficient of variation δ for the test series are given for all three choices of shear depth. The quantities z, h_s, and h_w are defined on Figure 1.2.1, and the values are read from Figure 2.2.2. N is the number of test results in each series. We note that the best agreement with the web crushing criterion, judging by the coefficient of variation, is obtained with the lowest value of shear depth. However, the difference can hardly be said to be striking.

Shear depth		$h^* = z$			$h^* = h_s$			$h^* = h_w$		
Series	N	z (mm)	ν (%)	δ (%)	h_s (mm)	ν (%)	δ (%)	h_w (mm)	ν (%)	δ (%)
T52	3	314	71.8	2.7	282	83.7	2.8	269	89.7	2.8
T60	15	314	71.8	5.7	282	81.6	6.0	269	86.6	6.2
T90	18	314	75.0	8.9	282	83.8	8.7	269	87.9	8.6
T52-60-90	36	314	73.9	7.4	282	83.2	7.3	269	87.7	7.2
Td	4	314	69.0	10.5	282	78.1	8.9	269	82.8	8.3
Tm	4	314	79.2	5.4	287	88.8	4.6	269	96.8	4.1

Table 5.4.1: Web effectiveness and coefficient of variation for different definitions of effective shear depth.

On Figures 5.4.1a and b, the test results for series T52, T60, and T90 combined (series T52-60-90) are plotted for $h^* = h_s$ and $h^* = h_w$, respectively. Comparing with Figure 5.2.1, we note no difference between the three graphs, except that in order to fit the experimental evidence, the web effectiveness must be changed according to the shear depth (cf. the following section).

Another indication of the effective shear depth may be obtained from the observations of stirrup yield. In the preceding section we found that the beams are overreinforced for $\psi > \psi_1$, where ψ_1 is bounded by the limits $0.37 < \psi_1 < 0.43$. According to the web crushing criterion, we have $\psi_1 = \nu/2$ (cf. Section 1.1), hence $0.74 < \nu < 0.86$, the upper limit being the most uncertain.

Comparing with Table 5.4.1, we deduce that the values $h^* = z$ and $h^* = h_w$ are just barely justified.

Thus neither the curve fitting nor the observations of stirrup yielding permit an exclusion of any of the three choices of shear depth. Indications are that the value $h^* = z$ is too great and $h^* = h_w$ is too small, and that it would be more correct to use the shear depth $h^* = h_s$, i.e. the distance between the bottom of the compression zone to the centroid of the lowest layer of main reinforcing bars enclosed by the stirrups. However, until more decisive experimental evidence is available, we must conclude that the choice of shear depth is principally a matter of taste.

a)

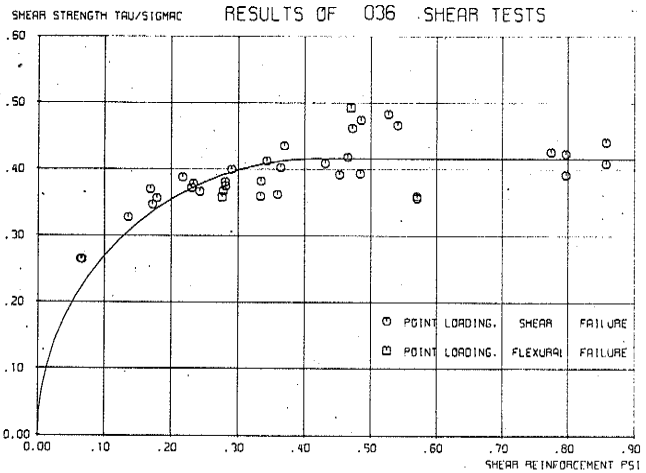

b)

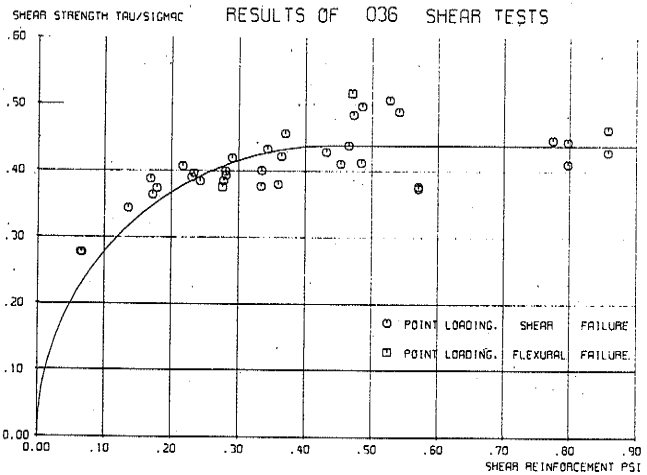

Figure 5.4.1: Test results for series T52, T60, and T90.

a) Shear depth : $h^* = h_s$

b) Shear depth : $h^* = h_w$

5.5 Effective web strength

From Table 5.4.1 it appears that the apparent web effectiveness is rather strongly dependent upon the choice of shear depth. This means that if the latter is reduced, the web effectiveness should be increased almost proportionally in order to yield the observed shear strength. As mentioned in the preceding section, the observations of stirrup yield indicate that the web effectiveness of all the beams of series T is greater than 74%.

The concentration of the web compression at the longitudinal bars, discussed in Section 1.2, might well be responsible for the fact that the effective web strength is less than the uniaxial compressive strength. In that case, the web effectiveness should be dependent upon stirrup layout and concrete cover. As explained in Section 2.2, the pilot series Td and Tm were included in order to shed light on this question, the differences from the normal beams being that series Td had three bars supported by stirrup bends, rather than two, and series Tm had only half the concrete cover. Consequently, we would expect an increase in web effectiveness for series Td and a reduction for series Tm. From Table 5.4.1, however, it appears to be the other way round.

The differences in web effectiveness observed may or may not be significant. This question is investigated comparing series Td and Tm with the rest of the beams, series T52-60-90, by the procedure used in Section 5.2. As before, the F-test reveals that the variances are not significantly different at the 95% level. The results of the t-test on the sample means are listed in Table 5.5.1, using the same notations as in Section 5.2.

Shear depth			$h^* = z$			$h^* = h_s$			$h^* = h_w$		
Series	N	$t_{97.5}$	s	s_{12}	t_{12}	s	s_{12}	t_{12}	s	s_{12}	t_{12}
Td T52-60-90	4 36	2.03	7.25 5.47	5.63	1.65	6.95 6.07	6.14	1.58	6.87 6.31	6.36	1.46
T52-60-90 Tm	36 4	2.03	5.47 4.28	5.39	1.87	6.07 4.08	5.94	1.79	6.31 3.97	6.16	2.80

Table 5.5.1: t-test on sample means

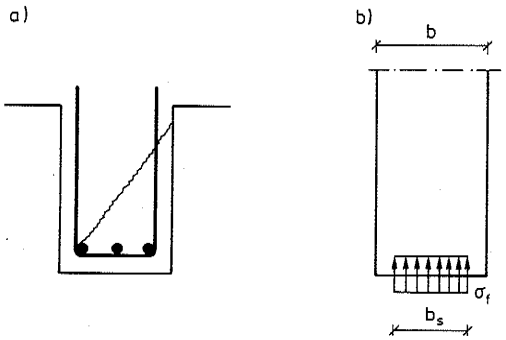

Figure 5.5.1: Web failure

a) Possible failure mechanism (normal section)

b) Web crushing idealized as strip load on prismatic concrete body. (inclined section)

From the table we note that the differences in web effectiveness between series Td and T52-60-90 are not significant at the 95% level ($t_{12} < t_{97.5}$). Series Tm is significantly if we put $h^* = h_w$, and almost so with $h^* = z$. If we explain the increase in shear strength of series Tm by an increase in shear depth by putting $h^* = h_s$, i.e. measuring the shear depth to the lower layer of reinforcing bars, then the observed difference in web effectiveness is far from significant.

These results suggest that the failure is not a local phenomenon at the longitudinal bars, but involves the entire web; cf. the discussion in Section 5.1. The web failure mechanism suggested by Figure 5.1.3 is shown on Figure 5.5.1a. The existence of oblique failure planes would explain the heavy crushing observed on the beam faces near the junction of web and flange, cf. Figures 4.2.1e and 4.2.2. Thus a tentative conclusion is that irrespective of the stirrup arrangement, the web strength is governed by the strength of the concrete body enclosed by the stirrups.

Adopting this point of view, the theoretical determination of the web strength is reduced to a plane problem. We consider a section parallel to the concrete struts, i.e. at the inclination φ with the beam axis, and idealize the action of the stirrups as a uniformly distributed strip load σ_f over the interior stirrup width b_s (see Figure 5.5.1b).

Data on concentrated loads on concrete prisms have been compiled by JENSEN [6], who concludes that the stress on the loaded area can be calculated by the formula (see also [7])

$$\frac{\sigma_f}{\sigma_c} = 0.2 + 0.8\sqrt{\frac{b}{b_s}} \quad ,$$

where b is the part of the supported area (width) which is symmetrical with respect to the centreline of b_s. Hence the web effectiveness is:

$$\nu = \frac{b_s \sigma_f}{b \sigma_c} = 0.2 \frac{b_s}{b} + 0.8 \sqrt{\frac{b_s}{b}} \qquad (3)$$

For the normal beams $b_s = 152$ mm and for series T_m $b_s = 176$ mm (cf. Figures 2.2.2a and c). Hence:

$$\nu = 0.2 \frac{152}{200} + 0.8 \sqrt{\frac{152}{200}} = 0.152 + 0.687 = 0.849$$

for the normal beams, and:

$$\nu = 0.2 \frac{176}{200} + 0.8 \sqrt{\frac{176}{200}} = 0.176 + 0.750 = 0.926$$

for series T_m.

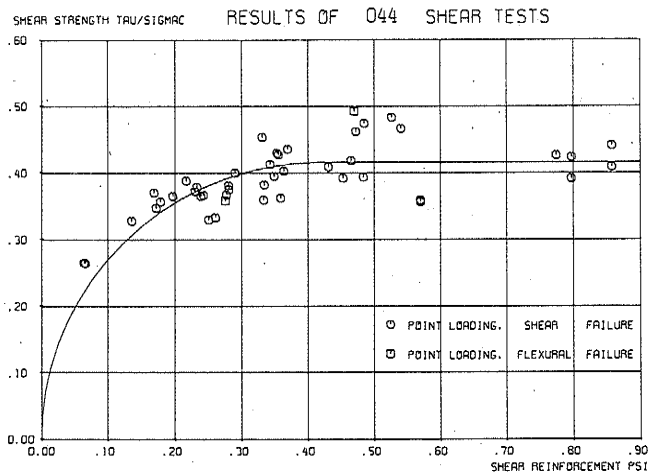

Figure 5.5.2: Test results for all the beams of series T (shear depth: $h^* = h_s$)

Comparing these values with those of Table 5.4.1, we note that they lie between the observed web effectiveness corresponding to $h^* = h_s$ and $h^* = h_w$.

From these considerations, two different provisional conclusions are possible:

1) The web effectiveness may safely be calculated by equation (3), provided the depth h_w of the web be used as shear depth.

2) The web effectiveness is independent upon the reinforcement arrangement. The depth h_s may be used as shear depth and the web effectiveness determined experimentally.

Obviously there is a limit to the web width for which any of these propositions is reasonable. Indeed, the conclusions will have to be reviewed in the light of the subsequent test series of the experimental programme.

On Figure 5.5.2, the results for all the beams of series T are plotted together, with h_s as shear depth. The web effectiveness is $\nu = 0.832$ with a coefficient of variation $\delta = 7.3\%$, the same as for series T52-60-90 alone (Table 5.4.1). If the web effectiveness does not depend on the stirrup arrangement, it must be governed by the limited deformability of the concrete, cf. the discussion in Section 1.2. In that case, we would expect the beams with the weakest concrete to have the highest web effectiveness. Inspection of the results shows that this is indeed the trend.

In Table 5.5.2, the 20 normal test beams failing in shear are grouped according to the individual web effectiveness. The centre column contains the beams where the strength of one shear span was below and the other above average, i.e. the two points are situated on either side of the curve on Figure 5.5.2. The left and the right column are the beams with both points (or the point in the case of only one shear failure) below or above the curve, respectively. The table lists the corresponding concrete strengths, and it appears that the highest strengths

Below average		Around average		Above average	
Beam Number	σ_c (kp/cm^2)	Beam Number	σ_c (kp/cm^2)	Beam Number	σ (kp/cm^2)
T 6032	120	T 5218	105	T 5214	109
T 9025	128	T 6022	106	T 6005	108
T 9040	115	T 6025	104	T 6010	105
T 9060	121	T 6029	108	T 6014	116
		T 9047	129	T 6018	112
		T 9071	111	T 9032	101
		T 9078	115	T 9036	107
				T 9043	105
				T 9065	102
Average	121	Average	111	Average	107

Table 5.5.2: Test results grouped according to individual web effectiveness.
(shear depth: $h^* = h_s$).

are associated with the lowest web effectiveness, and vice versa. A closer analysis shows that the difference in average concrete strength for the beams in the left and the right column is highly significant.

The flexural failures (Beams Nos.T5222 and T9025) have not been considered so far, but on Figure 5.5.2 it is noted that Beam No.T9029, which had a very low concrete strength, must have had a very high web effectiveness.

A theoretical prediction of the web strength would be most satisfactory. On the other hand, the web effectiveness for beams of a reasonable design seems to be fairly constant. In reference [3], the results of 153 shear tests reported in the literature have been plotted together, using the internal moment lever arm as shear depth ($h^* = z$) . The web effectiveness is $\nu = 0.72$ with a coefficient of variation of only 6%.

ACKNOWLEDGEMENTS

As explained in the introduction, the Danish Council for Scientific and Technical Research sponsored an experimental programme running from April 1973 to March 1976. The responsible leader of the project was Professor M.P.Nielsen in collaboration with Professor T.Brøndum-Nielsen and lecturer H.C. Sørensen of the Structural Research Laboratory. The actual testing of series T was carried out by M.W.Bræstrup.

Currently, the research project is executed by the authors of the present report, headed by Professor M.P.Nielsen. The group is occasionally joined by H.C.Sørensen, who now is Head of Department at the Concrete Research Laboratories at Karlstrup. Professor T.Brøndum-Nielsen has read the manuscript of the report and contributed with many valuable suggestions.

REFERENCES

[1] NIELSEN, M.P.:
Om forskydningsarmering i jernbetonbjælker. (On shear reinforcement in reinforced concrete beams).
Bygningsstatiske Meddelelser Vol.38, No.2. November 1967. pp.33-58.

[2] NIELSEN, M.P.:
Discussion on [1]
Bygningsstatiske Meddelelser. Vol.40, No.1. October 1969. pp.60-63.

[3] NIELSEN, M.P. & BRÆSTRUP, M.W.:
Plastic shear strength of reinforced concrete beams.
Bygningsstatiske Meddelelser. Vol.46, No.3. September 1975. pp.61-99.

[4] BRÆSTRUP, M.W.:
Plastic analysis of shear in reinforced concrete.
Magazine of Concrete Research. Vol.26, No.89, December 1974. pp.221-228.

[5] BRØNDUM-NIELSEN, T.:
Betonkonstruktioner I
Copenhagen, Technical University of Denmark, Structural Research Laboratory, 1969. pp.267.

[6] JENSEN, B.C.:
Koncentrerede belastninger på uarmerede betonprismer. (Concentrated loads on plain concrete prisms).
Bygningsstatiske Meddelelser. Vol.44, No.4. December 1974. pp.89-111.

[7] JENSEN, B.C. & NIELSEN, M.P.:
Om spalteforsøget og om koncentrerede kræfter på uarmerede betonprismer. (Splitting tests and concentrated loads on unreinforced concrete prisms).
Nordisk Betong. No.3, May 1975. pp.9-13.

[8] KEEPING, E.S.:
Introduction to statistical inference.
Princeton, N.J., D.van Nostrand Company, Inc., 1962. pp.451.

[9] DS F 32/74
Forslag til Dansk Standard: Betonkonstruktioner, prøvningsmetoder.
Copenhagen, Dansk Standardiseringsråd. 1974.

SUMMARY

The present report describes shear tests on 26 simply supported reinforced concrete beams which were loaded to failure in the term 1973/74 at the Structural Research Laboratory of the Technical University of Denmark. The test series is the first part of a research programme, sponsored by the Danish Council for Scientific and Technical Research. The test beams, with a T-shaped cross-section, had a span of 3 m and were subjected to two symmetrical point loads at a distance of 90 cm. The shear reinforcement consisted of vertical stirrups. The principal test variables were the amount of shear reinforcement (16 different values) and the strength of main reinforcement (3 values). The concrete strength was attempted at a constant value of approximately 11 MPa (110 kp/cm^2). A few pilot tests with different stirrup arrangements were included. 2 of the beams failed in flexion. For 20 beams, failure of both shear spans were achieved by two tests.

The theoretical background for the test series is an analysis based upon the theory of plasticity, and described in references [1]-[4]. The analysis is briefly summarized in Chapter 1. The theoretical solution for the ultimate shear load V is given by:

$$V = bh^* s_Y \sqrt{\frac{\nu\sigma_c}{s_Y} - 1} \qquad \text{for} \qquad s_Y \leq \frac{1}{2}\nu\sigma_c \tag{1a}$$

$$V = \frac{1}{2}bh^*\nu\sigma_c \qquad \text{for} \qquad s_Y \geq \frac{1}{2}\nu\sigma_c \tag{1b}$$

Here :

- b is the web width,
- h^* is the effective shear depth,
- s_Y is the strength (yield force) of the stirrups per unit area perpendicular to the stirrup direction,
- σ_c is the concrete cylinder strength,
- ν is a web effectiveness factor

The corresponding stress state and failure mechanism are described in Section 1.1 (cf. Figure 1.1.1).

Equations (1) are termed the web crushing criterion, because the ultimate load corresponds to the situation that the inclined web compression reaches the concrete strength limit. The formulae contain two empirical parameters, viz. h^* and ν. h^* is the depth of the concrete body which is effective in the resistance of shear stresses. The Danish Code of Practice, DS 411, puts $h^* = z$, z being the internal moment lever arm. This value is used as the starting point by the analysis of the test results. There are other alternatives, however, as indicated in Section 1.2. ν is a parameter which describes the efficiency of the web concrete in resisting the inclined compression. Presumably, ν depends upon various factors, including the reinforcement layout and the concrete deformability.

The object of the test series was to investigate the applicability of the analysis described above. As mentioned in Section 2.1, the purpose is laid down in the following points:

(1) To verify that the failure mechanism is a pure shear deformation, without any rotation of the beam end (cf. Figure 1.1.1)

(2) To verify that the ultimate shear load is independent of the strength of main reinforcement, provided the latter is sufficient to ensure shear failure

(3) To verify that with sufficiently strong shear reinforcement, the ultimate load is independent of the shear reinforcement degree (cf. equation (1b))

(4) To determine the shear depth h^* and the web effectiveness ν.

Chapter 2 further contains a description of the test beams, their reinforcement, and their flexural capacities.

The execution of the tests, including the testing of concrete and reinforcement, is described in Chapter 3. A fairly thorough review of test procedure and equipment is given, since these are used almost unchanged at the subsequent series of the experimental programme. The actual beam testing differs from usual shear tests by the fact that the rotation of one beam end over the support is measured.

Chapter 4 describes the test results. The ultimate loads obtained are listed in Table 4.2.1. The numerical analysis of the results, including the plotting of curves, is carried out on electronical computer.

In Chapter 5 the conclusions of the test series are stated. The principal points are as follows:

(1) The behaviour of the beams under loading to failure is essentially as predicted. A marked decrease in the inclination of newly formed cracks is observed as the load increases. The previous cracks are transformed into yield lines carrying shear. It turns out that yield lines are formed in the concrete before the stirrups are yielding. The failure mechanism is as assumed, at failure there is no rotation of the beam end. A cutting through of two beams after failure shows, rather surprisingly, that the cracks appearing on the beam faces do not penetrate the web. It seems that the web failure occurs along planes that are not perpendicular to the plane of the beam.

(2) No significant difference is observed between the ultimate shear loads of beams with different strengths of main reinforcement. Two of the beams had yielding in the bending span, with no apparent influence upon shear strength.

(3) Four beams with very strong stirrup reinforcement ($s_y > \frac{1}{2}\sigma_c$) achieved approximately identical ultimate loads. In other respects, the behaviour of these beams was essentially the same as of the rest.

(4) An analysis of the test results to determine the shear depth h^* does not permit a rejection of the value $h^* = z$, although it seems a bit on the high side. The web effectiveness giving closest fit to the test results is highly dependent upon the choice of h^*. With $h^* = z$ we get $\nu = 0.74$ with a coefficient of variation of 7.4%. A calculation of ν based upon analysis of concentrated loads on concrete prisms yields values that are two great, unless a smaller shear depth is used. The pilot tests do not show any major influence of the reinforcement lay-out. However, there is a significant decrease of ν with increasing concrete strength.

DANSK RESUMÉ

Den foreliggende rapport beskriver forskydningsforsøg med 26 simpelt understøttede jernbetonbjælker, som blev udført i året 1973/74 på Afdelingen for Bærende Konstruktioner ved Danmarks tekniske Højskole. Forsøgsserien udgør første del af et treårigt forskningsprojekt med støtte fra Statens teknisk-videnskabelige Forskningsråd. Forsøgsbjælkerne spændte 3 m, havde T-formet tværsnit og belastedes med to symmetriske enkeltkræfter med afstanden 90 cm. Som forskydningsarmering benyttedes lodrette bøjler. Ved forsøgene varieredes forskydningsarmeringsintensiteten (16 forskellige værdier) og styrken af hovedarmeringen (3 værdier), mens betonstyrken søgtes holdt konstant på en værdi af ca 11 MPa (110 kp/cm^2). Der blev udført enkelte vejledende forsøg med forskellige bøjlearrangementer. To af bjælkerne fik bøjningsbrud. For 20 bjælker opnåedes brud i begge forskydningsfag ved udførelse af to forsøg.

Den teoretiske baggrund for forsøgsserien er en beregningsmodel baseret på plasticitetsteorien. Modellen er kort beskrevet i Kapitel 1, men i øvrigt henvises til referencerne [1]-[4]. Den plasticitetsteoretiske løsning for forskydningsbæreevnen V er givet ved:

$$V = bh^* s_Y \sqrt{\frac{\nu\sigma_c}{s_Y} - 1} \qquad \text{for} \qquad s_Y \leq \frac{1}{2}\nu\sigma_c \qquad (1a)$$

$$V = \frac{1}{2}bh^*\nu\sigma_c \qquad \text{for} \qquad s_Y \geq \frac{1}{2}\nu\sigma_c \qquad (1b)$$

Her er:

- b : Bjælkens kropbredde
- h^* : Bjælkens forskydningshøjde
- s_Y : Styrken (flydekraften) af bøjlerne pr arealenhed af et snit vinkelret på bøjleretningen
- σ_c : Betonens cylinderstyrke
- ν : Effektivitetsfaktor for bjælkekroppen

Den til løsningen hørende spændingstilstand og brudmekanisme er beskrevet i Afsnit 1.1 (se Figur 1.1.1).

Ligningerne (1) benævnes trykbrudskriteriet, fordi bæreevnen anses at være udtømt, når og først når det skrå betontryk i bjælkekroppen overstiger betonens styrke. Formlerne indeholder to empiriske parametre, nemlig h^* og ν. h^* er højden af det betonlegeme, som kan regnes effektivt ved optagelse af forskydningsspændingerne. Den danske betonnorm, DS 411, regner $h^* = z$, hvor z er bjælkens indre momentarm, og det er den værdi, som benyttes som udgangspunkt ved behandling af forsøgsresultaterne. Som angivet i Afsnit 1.2, kan der imidlertid tænkes andre muligheder. ν er en parameter, som beskriver, hvor effektiv bjælkekroppen er til optagelse af det skrå betontryk. ν må forudses at afhænge af en række faktorer, herunder armeringsarrangementet og betonens flydeevne.

Hensigten med forsøgsserien var at undersøge anvendeligheden af ovennævnte beregningsmodel. Som nævnt i Afsnit 2.1, er formålet udmøntet i følgende punkter:

(1) Verifikation af at brudmekanismen er en ren forskydningsdeformation uden rotation af bjælkeenden (sml. Figur 1.1.1).

(2) Verifikation af at forskydningsbæreevnen er uafhængig af hovedarmeringens styrke, forudsat at denne er tilstrækkelig til at sikre forskydningsbrud.

(3) Verifikation af at når forskydningsarmeringen er tilstrækkelig stærk, er bæreevnen uafhængig af forskydningsarmeringsgraden (sml. ligning (1b)).

(4) Bestemmelse af forskydningshøjden h^* og effektivitetskoefficienten ν.

Kapitel 2 indeholder desuden en beskrivelse af forsøgsbjælkerne, deres armering og bøjningsstyrker.

Forsøgenes udførelse, herunder prøvning af beton og arme-

ring, er beskrevet i Kapitel 3. Der er givet en temmelig grundig gennemgang af måleudstyr og forsøgsprocedure, idet disse benyttes nogenlunde uændret ved de følgende serier i forsøgsprogrammet. Selve bjælkeprøvningen adskiller sig fra sædvanlige forskydningsforsøg derved, at der er foretaget målinger af den ene bjælkeendes rotation over understøtningen.

Kapitel 4 beskriver forsøgsresultaterne. De fundne brudlaste er opført i Tabel 4.2.1. Den numeriske behandling af resultaterne, herunder optegning af kurver, er foretaget på datamat.

I Kapitel 5 er konklusionerne af forsøgsserien gennemgået. Hovedindholdet er som følger:

(1) Bjælkernes opførsel under belastning til brud er stort set som antaget. Der konstateres en tydelig formindskelse af de nydannede revners hældning, når belastningen vokser. De ældre revner omdannes til brudlinier, som overfører forskydningsspændinger. Det viser sig, at der dannes brudlinier i betonen, før der er flydning i bøjlerne. Brudmekanismen er som forudsat; ved brud sker der ingen rotation af bjælkeenden. En gennemskæring af to bjælker efter brud viser temmelig overraskende, at de revner, der ses på bjælkens sider, ikke forplanter sig igennem kroppen. Derimod synes det, som om bruddet i bjælkekroppen sker langs planer, som ikke er vinkelret på bjælkens plan.

(2) Der konstateres ingen signifikant forskel på forskydningsbæreevnerne af bjælker med forskellige styrker af hovedarmeringen. To af bjælkerne opnåede flydning i bøjningsfaget, hvilket tilsyneladende ikke påvirkede forskydningsstyrken.

(3) Fire bjælker med meget kraftig bøjlearmering ($s_Y > \frac{1}{2}\sigma_c$) opnåede stort set samme brudlast. I øvrigt var opførslen af disse bjælker ikke væsensforskellig fra restens.

(4) En behandling af forsøgsresultaterne med henblik på en bestemmelse af forskydningshøjden h^* giver ikke grundlag for at afvise værdien $h^* = z$, omend den synes at være noget i overkanten. Den effektivitetsfaktor ν, som stemmer bedst med forsøgsresultaterne, er stærkt afhængig af valget af h^*. Med $h^* = z$ fås $\nu = 0.74$ med en variationskoefficient på 7.4%. En beregning af ν på grundlag af en analyse af koncentrerede belastninger på betonprismer giver værdier, som er for store, medmindre man anvender en mindre forskydningshøjde. De vejledende forsøg tyder ikke på, at armeringsarrangementet har nogen større indflydelse på ν. Derimod er der en tydelig tendens til, at ν aftager med voksende betonstyrke.

AFDELINGEN FOR BÆRENDE KONSTRUKTIONER
DANMARKS TEKNISKE HØJSKOLE

Structural Research Laboratory
Technical University of Denmark, DK-2800 Lyngby

RAPPORTER (Reports)
(1974 -)

R 43. BORCHERSEN,EGIL: Moiré pattern deformation theory and optical filtering techniques. 1974.
R 44. BRØNDUM-NIELSEN,TROELS: Optimum design of reinforced concrete shells and slabs.
R 45. PEDERSEN,FLEMMING BLIGAARD: Dynamic properties of anti-vibration mountings. 1974.
R 46. PHILIPSEN,CLAUS: Interferensholografisk bestemmelse af legemers form og flytningsfelt. 1974.
R 47. LARSEN,H.J. og H.RIBERHOLT: Tværbæreevne af søm og dykkere i spån- og træfiberplader. 1974.
R 48. POULSEN,P.E.: The photo-elastic effect in three--dimensional states of stress. 1974.
R 49. NIELSEN,J.: Modellove for kornede medier med særligt henblik på silomodeller. 1974.
R 50. KRENK,STEEN: The problems of an inclined crack in an elastic strip. 1974.
R 51. BRØNDUM-NIELSEN,TROELS: Effect of prestress on the damping of concrete. Effect of grouting on the fatique strength of post-tensioned concrete beams. 1974.
R 52. EGERUP,ARNE RYDÉN,H.J.LARSEN,H.RIBERHOLT and ERIK SØRENSEN: Papers presented at IUFRO-V, International Union of Forestry Research Organisation, Division V, Congress 1973. 1974.
R 53. HOLST,OLE: Automatic design of plane frames. 1974.
R 54. NIELSEN,SØREN: Svingninger i mastebarduner. 1974.
R 55. AGERSKOV,HENNING: Behaviour of connections using prestressed high strength bolts loaded in tension. 1974.
R 56. MØLLMANN,H.: Analysis of prestressed cable systems supported by elastic boundary structures. 1974.
R 57. NIELSEN,J. and V.ASKEGAARD: Scale errors in model tests on granular media with special reference to silo models. 1974.
R 58. SVENSSON,SVEN EILIF: Stability properties and mode interaction of continuous, conservative systems. 1974.
R 59. SIGBJÖRNSSON,RAGNAR: On the theory of structural vibrations due to natural wind. 1974.
R 60. SØRENSEN,HANS CHR.: Shear tests on 12 reinforced concrete T-beams. 1974.

R 61. NIELSEN,LEIF OTTO: Spændingshybride finite elementer til svingningsproblemer. 1975.
R 62. EGERUP,ARNE RYDÉN: Theoretical and experimental determination of the stiffness and ultimate load of timber trusses. 1975.
R 63. LAURSEN,MARTIN: A curved beam equilibrium element applicable in standard finite element program systems. 1975.
R 64. BACH,FINN: Metoder til måling af egenspændinger. 1975.
R 65. BACH,FINN: En teoretisk og eksperimentel undersøgelse af den akustoelastiske metodes anvendelighed til egenspændingsmåling. 1975.
R 66. PEDERSEN,FLEMMING BLIGAARD: Measurement of the complex modulus of viscoelastic materials. 1975.
R 67. PEDERSEN,FLEMMING BLIGAARD: Svingningsforsøg med viskoelastisk dæmpede sandwichbjælker. 1975.
R 68. AGERSKOV,HENNING: Analysis of high strength bolted connections subject to prying. A simplified approach. 1975.
R 69. PEDERSEN,MAX ELGAARD: En 2.ordens tilnærmelse til de konstitutive ligninger for beton. 1976.
R 70. RIBERHOLT,HILMER, and PETER CHR. NIELSEN: Timber under combined compression and bending stress. 1976.
R 71. KRENCHEL,HERBERT og J. BJØRNBAK-HANSEN: Undersøgelse af let konstruktionsbetons væsentligste materialeparametre. 1976.
R 72. FRÆSTRUP,M.W., M.P. NIELSEN, FINN BACH and B.CHR. JENSEN: Shear Tests on Reinforced Concrete T-Beams. Series T. 1976.